NSG-7264

Netherlands foundation for radio-astronomy

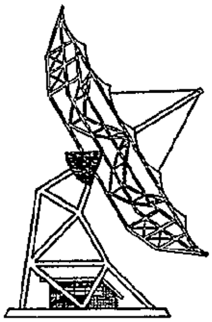

(NASA-CR-156129) MAPS OF JOVIAN RADIO EMISSION Final Technical Report, 1 Oct. 1976 - 1 Oct. 1977 (Leiden Univ.) 57 p HC A04/MF A01 CSCL 03B

N78-21032

Unclas G3/91 11876

Stichting radiostraling van zon en melkweg

RADIOSTERRENWACHT DWINGELOO
Dwingeloo Nederland
Telefoon 05219-7244 - Telex 42043

RADIOSTERRENWACHT WESTERBORK
post Hooghalen Nederland
Telefoon 05939-421 - Telex 53621

Final Technical Report concerning:

MAPS OF JOVIAN RADIO EMISSION

Imke de Pater

Grant no. NSG-7264

period covered by the report: Oct. 1 1976 - Oct. 1 1977

P.I: H. van der Laan , Professor

name institution: Leiden University

address: Leiden 2405 Netherlands
Department of Astronomy

Chapter I. The telescope.

The Westerbork radiotelescope is an earth-rotation aperture synthesis array; it consists of (at the time of the observations!) 12 equally spaced antennae on an E-W line of which two are moveable along a railway track. The diameter of each antenna is 25 m.

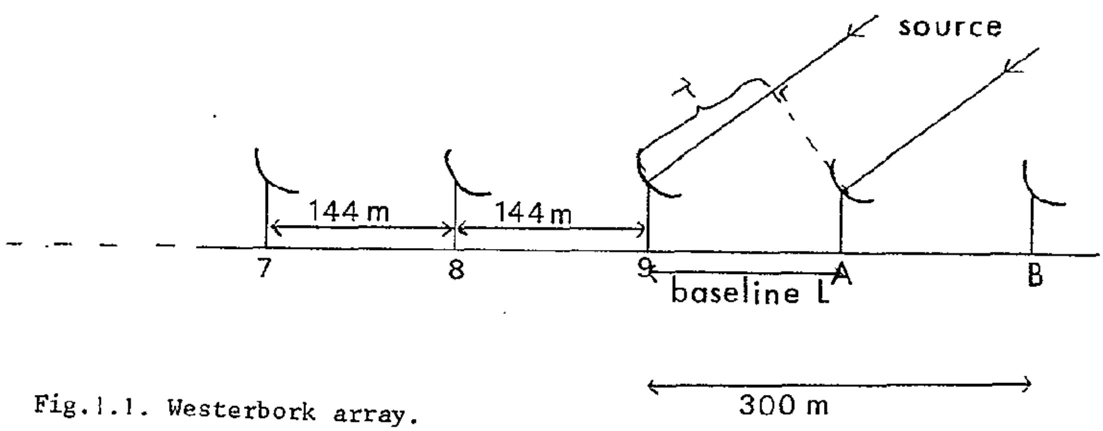

Fig.1.1. Westerbork array.

The elements are all equiped with a dual-polarization frontend, so that all 4 Stokes parameters can be measured simultaneously. There are three frequencies available: 610 MHz, 1415 MHz and 4995 MHz. Each of the two moveable antennae forms an interferometer with each of the 10 fixed antennae: thus when we observe a source we use simultaneously 20 interferometers each with a different baseline length L_i and a resolution λ/L_i' radians, where L_i' is the projected baseline length: projected onto a plane perpendicular to the direction of the source. (This plane is called the UV plane).

As the earth rotates these projected baselines trace out ellipses in the UV plane (with the small axis $b = L_i \sin \delta$) which gives us the possibility to build up in 12 hr. a two-dimensional picture of the sky which shows us both the large and small scale structures of the source. (technique of aperture synthesis, see: Ryle and Hewish, 1960; Ryle, 1962) Suppose that we have an interferometer with a spacing (u,v) in the UV plane; the two antennae receive identical correlated signals from a point in the source on a distance (l,m) from the center of the observed region, except for a difference in arrival time of the waves due to a difference in pathlength (ul + vm). The terms l and m are direction cosines with respect to the center of the observed region at (α_o, δ_o)

$$\left(l = -\sin \Delta\alpha \cos \delta \ ; \quad m = \frac{\cos \delta_o + \cos\Delta\alpha \cos\delta}{\sin \delta_o} \right)$$

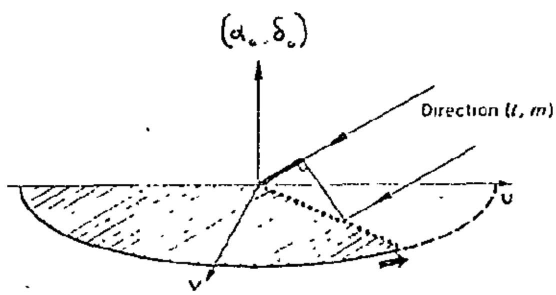

Fig.1.2.

If U and V are expressed in λ we can write the difference in arrival time of the waves as a phase difference $\psi = 2\pi$ (ul + vm). The Westerbork receiver measures the time averages of $A \cos \psi$ and $A \sin \psi$ (with an integration time of 30 sec) where A is proportional to the correlated output power from the individual antennae. We can write the complex receiver output as:

$$\Delta W = A \cos \psi + i A \sin \psi = A \exp (i \psi) \tag{1}$$

where $A \sim \Delta\Omega . P . T_b$
T_b = brightness temperature T_b (l,m)
P = individual antenna pattern P (l,m)
$\Delta\Omega$ = solid angle = dldm/sin δ

The receiver output then can be written as a Fourier relation:

$$W(u,v) = \iint_{-\infty}^{+\infty} \left\{\frac{\text{const}}{\sin \delta} PT_b\right\} \exp \left[i.2\pi \; (ul + vm)\right] \; dldm \tag{2}$$

and, since T_b is real, $W(-u,-v) = W^{*}(u,v)$ where $*$ indicates the complex conjugate. Thus observing a source during 12 hours gives us a full coverage of the UV plane. Inverting this relation we get the spatial brightness distribution T_b (l,m) of the observed region (Högbom and Brouw, 1974). However we don't measure from infinity to infinity as the integral indicates since we have a finite aperture distribution; moreover it is possible that we might observe only a few hours instead of the 12 hours needed to fill the UV plane completely. We therefore write the receiver output W as W.g where g is a grading function equal to zero at all spacings at which there are no measurements and equal to a chosable value $0 < g \leq 1$ at all other spacings. Inverting the Fourier relation then we get the brightness distribution of the sky convolved with the synthesized beam pattern of the telescope:

$$\left\{\frac{const}{\sin\delta} . P . T_b\right\} * G = \int\int_{-\infty}^{+\infty} W.g \exp\left[-i.2\pi(ul + vm)\right] du\, dv \quad (3)$$

where G is the Fourier transform of g and is called the synthesized beam; fo the case of a uniform aperture distribution and a full 12 hr. observation we have a synthesized beam with a -13% first sidelobe (see fig.1.3); for the truncated gaussian grading (tapered to 25% at maximum baseline), normally used in Westerbork reduction programmes, the beam has only a -5% first side-lobe for a full 12 hr. observation (Brouw, 1971).

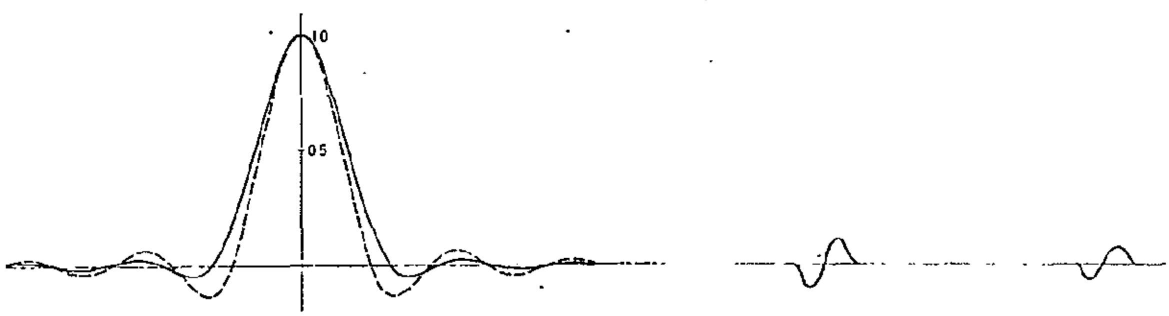

Fig.1.3.Crossection of the synthesized beam including the closest two grating rings. The solid line gives the pattern for the standard Westerbork gaussian grading; the dashed curve shows the somewhat narrower beam with larger sidelobes that can be obtained with a uniform grading.

Furthermore, the discrete nature of the synthesized aperture causes diffractio grating rings centered around the source with radii $\Delta l = \frac{1}{\Delta u}$ and $\Delta m = \frac{1}{\Delta u} \sin\delta$. A map of the sky after a 12 hr. observation is shown in fig. 1.4. It is obvious that one wants to get rid of the distortions in the map due to the synthesized beam pattern of the telescope, particularly in the case of large unobserved portions of the UV plane (compare Jupiter, fig.3.3) this can be done with help of a deconvolution technique such as "clean" developed by Högbom (1973). (Chapter III.3 describes this technique in more detail).

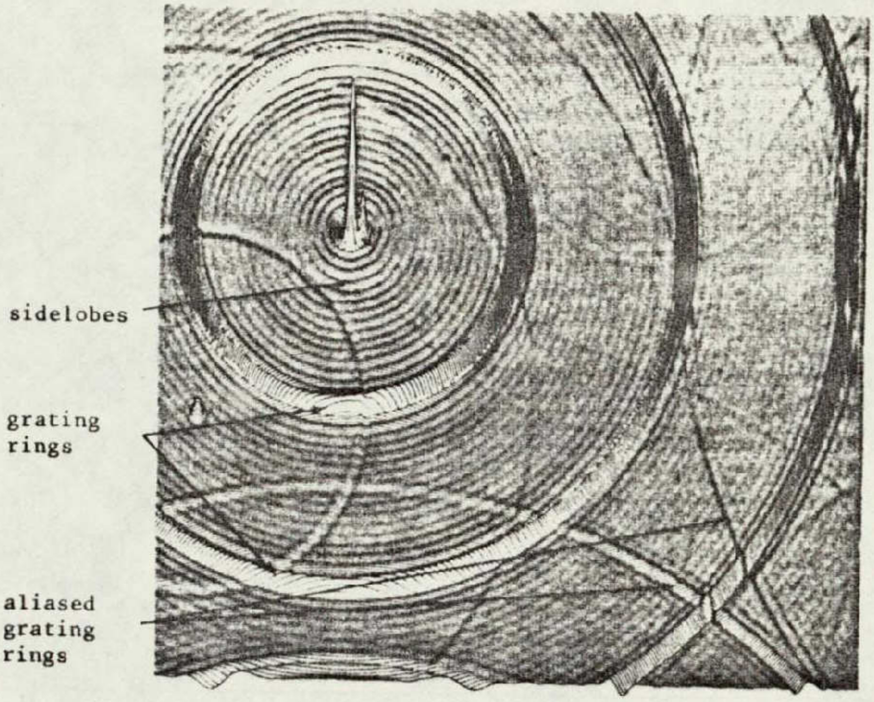

Fig.1.4. portion of a typical Westerbork map after a full 12 hr. synthesis.

In this short derivation of the Fourier relation (3) we have ignored several effects of consequence to a working interferometer as there are i.e. the finite bandwidth and delay tracking system:

-The interferometer system is of course not monochromatic as was tacitly assumed in the derivation of the Fourier relation, but has a finite bandwidth (in effect as wide as possible to obtain a high sensitivity). The produced map in that case will be the same map but radially smeared with a function $\frac{\Delta v}{v_o}$ .d, where Δv = bandwidth with centre frequency v_o and d = distance to the centre of the map. In Westerbork Δv = 4.2 MHz which will give a smearing effect of 6" at 21 cm for a source 0°.5 away from the field center.

— The radiation an interferometer receives from a point in the sky arrives at the two antennae with a time-delay $\tau = \frac{B}{c} \cos \theta$ (t) (see fig. 1.1). The rotation of the earth causes θ to vary with time. The response of an interferometer then can be pictured as a set of fixed quasi-sinusoidal fringes in the sky through which the radiosource travels; the receiver output W shows a quasi-sinusoidal response to this source: $W(t) \sim T_b \cos (\frac{2\pi B}{\lambda} \cos \theta\ (t))$. To reduce the amount of data we get from this source the integration time must be as large as possible but at the same time small with respect to the fringe-pattern of the telescope. In Westerbork an integration time of 30 sec. can be tolerated by using a so called "fringe stopping" technique: the output of the correlator is mixed with a frequency corresponding to the fringe frequency of a specific position on the sky, the socalled fringe stopping center (this is in general the center of the observed region).
However, as said before the telescope does not work monochromatically with frequency v_o for which the fringe stopping is done, but there is a band pass of frequencies $(v-v_o)$ and for these frequencies the fringe stopping center will be displaced which causes a loss of correlation. There is no problem if the fringe stopping can be done with a frequency dependent mixer or continuously varying time delay; in Westerbork pieces of cable length are inserted from the antenna receiver to the correlator to compensate for this time delay τ. The non continuous changes $\Delta\tau$ in delay produce phase errors $\Delta\phi = \Delta\tau\ (v - v_o)$; as long as $\Delta\tau \ll \frac{1}{\Delta v}$ the receiver operates allright. The delay tracking system in Westerbork is such that the loss of correlation due to the timedelay is not more than 1.5%.

(For further details see Casse and Muller, 1974 and Brouw, 1975).

Table 1. Mechanical data of the Westerbork array (for further details see Baars and Hooghoudt, 1974)

Spacing between the fixed position antennas	144 m
Length of rail for the movable antennas	300 m
Minimum available interferometer spacing	36 m
Maximum available interferometer spacing	1602 m
Diameter of the parabolic reflectors	25 m
Steerable in hour angle	$\pm 6^h$ from the meridian
Steerable in declination	$+90°$ to the horizon
Pointing accuracy in RA[a])	± 0.01 degree
Surface	8 mm mesh, 0.8 mm steel wire
Surface accuracy	1.4 mm rms

[a]) The pointing accuracy in declination has not been quite satisfactory, but steps have been taken to improve the performance.

Table 2. Telescope performance data with present receivers after one 12 hour measurement (for further details see Casse and Muller, 1974)

	Frequency MHz		
	610	1415	4995
Antenna aperture efficiency	0.59	0.54	0.44
Antenna half-power beamwidth (field of view)	83′	36′	11′
Synthesized beam, half-power beamwidth (in RA)	56″	24″	6″8
Radius of closest grating ring (in RA)	23′	10′	2′8
System noise temperature, K	400	260	200
Receiver equivalent bandwidth, MHz	4.2	4.2	4.2
Sensitivity[a]) $(\Delta S)_{rms}$, mfu[b])	1.0	0.9	0.9
Sensitivity[a]), $(\Delta T)_{rms}$, K/sin δ	1.3	1.2	1.2

[a]) Theoretical values. The fluctuations are generally found to be somewhat higher and to be influenced by the meteorological conditions.
[b]) 1 mfu = 10^{-29} W m^{-2} Hz^{-1}.

ORIGINAL PAGE IS
OF POOR QUALITY

References.

Baars, J.W.M., Hooghoudt, B.G. 1974, Astron. & Astrophys. 31, 323.

Brouw, W.N. 1971 Thesis

Brouw, W.N. 1975, Methods in Comput. Phys. 14, 131

Casse, J.L., Muller, C.A. 1974, Astron. & Astrophys. 31, 333

Fomalont, E.B., Wright, M.C.H. 1973, in Galactic and Extragalactic Radio Astronomy, Ed., G.L. Verschuur and K.I. Kellermann, Springer-Verlag.

Högbom, J.A. 1974, Astron. & Astrophys. Suppl. 15, 417.

Ryle, M. and Hewish, A. 1960, Monthly Notices Roy. Astron. Soc. 120, 220

Ryle, M. 1962, Nature, 194, 517.

Chapter II. Reduction of observations.

The data we get with the Westerbork telescope from a region of the sky have to be corrected for phase and amplitude errors before fourier transforming them into a brightness distribution of the sky. In this chapter the various sources of phase and amplitude errors are described; with help of the standard reduction program MAKEOBS (and/or REMOBS) one can correct the raw measurements for these errors. (For more details see Internal Technical Report ITR.78 of the NFRA; Brouw, 1971 or 1975). The goal in developing these correction programs was to attain a phase accuracy of 1^{o} and a gain stability of about 2%; calibrations show that this indeed can be obtained.

a) position variations

All data are corrected for changes in the apparent coordinates due to

- refraction
- precession
- nutation
- aberration (diurnal and annual)

Precise refraction can only be calculated if the actual properties of the atmosphere are known, at any position and time. Therefore these corrections are idealized, based on a model atmosphere consisting of a homogeneous shell around the earth with a thickness of 8000 m; the radiation rays inside the atmosphere were assumed to be parallel. The maximum changes in phase at certain zenith angles, z, can be found in the following table.

z	Δφ (21cm)	Δφ (6 cm)
0°	0°	0°
20°	0.4°	1.4°
40°	1.2°	4.2°
60°	3.8°	13.4°
80°	34.0°	120°

Up to a zenith angle z of about 70-75° there will be no great troubles at 21 cm doing a full synthesis ($\delta \sim 20^\circ$ to 26° at hourangle 90°).

b) errors dùe to atmospheric extinction

The extinction of the radiation in the atmosphere will decrease the source intensity with a factor exp (-K.F(z)) where K = extinction coëfficient, F(z) = normalized air mass function, assumed to be equal to $\frac{1}{F_o} \int_z \rho ds$.
One can derive (Kraus 1966):

$$I_{true} = I_{obs}\ G \sqrt{T_{RT}} \{1+PF\ (z)\} \qquad (1)$$

I_{true} = intensity of the source
I_{obs} = observed intensity
G = Gain factor
T_{RT} = receiver temperature
P = $-\frac{kT_{atm}}{2T_{RT}}$ with T_{atm} = atmospheric temperature

ORIGINAL PAGE IS OF POOR QUALITY

With F(z) being equal to sec (z) the coefficients P and K were determined experimentally by total power measurements and calibration observations as a function of z.

Frequency	P	K
4995 MHz	0.0083 ± 0.0075	-0.0365 ± 0.0075
1415 MHz	0.0046 ± 0.0025	-0.0146 ± 0.0025
610 MHz	–	–

c) faraday rotation in the ionosphere

For polarization measurements the faraday rotation χ in the ionosphere is equal to:

$$\chi = 1.36 \times 10^{6}\ n_t \bar{B}\ \nu^{-2} \quad \text{(in degrees)}$$

where n_t = total electron content , cm^{-2}

$\bar{B}$ = mean geomagnetic field along the line of sight

ν = observing frequency

The information about n_t comes from the Royal Dutch Meteorological Institute in the Bilt. The rotation angles are calculated with help of a computer program written by R. Strom which calculates $\bar{B}$ in the direction of the source.

The 50 cm observations in particular have to be corrected for this rotation; at 21 cm χ is only a few degrees and hardly shows any change during the measurements. It only gives then a systematic offset in the position angles of the polarization.

d) clock, frequency and baseline errors

It is assumed during the observations that the phase centers of all telescopes lie on a straight line exactly East-West. This is not true due to a constant offset of the phase centers from the perfect East-West line and to a misalignment of the polar axis of each element (which causes the line between the phase centers to vary in length and direction during the measurement). Corrections are determined from a lot of measurements of the calibration sources listed in table I, with the assumed positions listed there.

Table I

source	RA	DEC	Flux 6 cm	Flux 21cm	Flux 50cm
3C147	84.68126	49.82858	8.18	21.57	37.78
3C48*	23.70761	32.90573	5.80	15.70	28.55
3C309.1*	224.73602	71.86977	3.84	8.12	13.51

* The fluxes of 3C48 and 3C309.1 are derived from the flux 3C147.

e) primary beam corrections

If a source is large in angular extent in comparison to the field of view (say 3' at $\lambda = 6$ cm) the radiation at the edges is attenuated due to the primary beam, which is the beam pattern of the individual telescopes; this effect is determined empirically and the data can be corrected for it.
A problem in connection with this beam arises when the optical axes of the individual elements of the array are not identically (that is within $0\overset{\circ}{.}01$) pointed at the coordinates of the source; in that case the radiation each antenna receives from the sources is attenuated due to its own primary beam. A correction needed for this would be a very complicated field-dependent correction which is not provided in the existing software.

f) <u>telescope overlapping errors</u> (shadowing effect)

If the telescopes are observing parts of the sky near the East and West baseline poles some telescopes will partly observe another antenna instead of the sky; errors caused in this way are on axis mainly gain errors which are determined empirically and can be applied as correction.

g) <u>receiver errors</u>

After the data are corrected for all possible errors mentioned above we assume that the remaining errors are (mainley) due to the receiver system. To correct also for these errors we have to calibrate the observations with socalled calibration sources, which are point sources with known position, flux and hopefully zero polarization ; the sources regularly used in Westerbork are the same sources listed in Table I with which the baseline errors were determined.

This phase and amplitude calibration of the whole telescope is performed regularly, a few times each day.

References

Brouw, W.N. 1971, Thesis

Brouw, W.N. 1975, Methods in Comput. Phys. 14, 131

Kraus, J.D., 1966: Radio astronomy. McGraw-Hill Book Company, New York.

Van Someren Greve, H.W., 1974, Astron. & Astrophys. Suppl. 15, 343

Weiler, K.W., 1973, Astron. & Astrophys. 26, 403

Internal Technical Report ITR 78.

Chapter III. Jupiter data.

In Nov-Dec. 1973 observations were made of Jupiter with the Westerbork telescope at all three frequencies available:

610 MHz : 8 x 1^{hr}

1415 MHz : 3 x $7^{hr}47^{m}$

4995 MHz : 5 x $7^{hr}47^{m}$

2 x ∿ 5^{hr}

The conditions under which the planet was observed are shown in table I, together with the conditions of this planet in December 1977.

In 1973 Jupiter was just above the horizon and in that part of the sky we expect a lot of atmospheric disturbances which will lead to a poor calibration of the data (see Ch. II a, b); moreover the planet was visible for only 7 hr. while a full synthesis requires 12 hr. In general therefore we do not make observations in this part of the sky but since it was just the time of the Pioneer 10 flyby we still decided to try it; I must admit however that the results we finally got from these data are nevertheless quite reasonable.

As a comparison, the conditions of the planet in December 1977 are given. This is an optimal time to observe this planet again; the planet has reached its maximum northerly declination and is in opposition to the earth.

Table I. conditions of Jupiter in December 1973 and December 1977.

	Dec. 1973	Dec. 1977
Dec.	-20^{o}	$+23^{o}$
Distance Earth-Jupiter	5.5 AU	4.5 AU
Disk diameter	36"	47"
Synthesis of	7 hr	12 hr

3.1 Reduction of the data.

In this section the corrections we applied to the Jupiter data are indicated together with the specific problems we had at the various wavelengths during the measurements. Finally the "tricks" used to cope with a moving and rotating object are described.

a. The raw measurements were first corrected for the errors described in Ch. II : position errors, atmospheric extinction (21 and 6 cm), Faraday rotation (50 cm), clock, frequency and baseline errors and errors due to a shadowing effect (partially! see Ch. II).
Primary beam corrections were not necessary since the Jovian emission region is much less than the field of view at all three frequencies.
We finally defined the phase and amplitude corrections: to diminish calibration errors due to the low declination of Jupiter we used the point source NRAO 530 (RA = 262.55614 and DEC = -13.04609) together with the three sources listed in Ch. II table I to determine the phase errors at 6 and 21 cm; at 50 cm only the three sources 3C147, 3C48 and 3C309.1 were used. The fixed gain factors were defined at all three wavelengths with help of the flux of 3C147.

b. The reduction steps which had to be taken after these "standard" corrections are described separately for all three wavelengths:
21 cm Fourier transforming the data into a brightness distribution of the sky gives us a picture of the field of view including the planet as shown in Fig. 3.1. It will be clear that background sources with their synthesized beam pattern (particularly the grating rings) greatly disturb the Jovian signal. Defining the position and flux of these background sources (with help of a computer program SEARCH, which approximates the sources as "point sources") one can subtract the response to these sources from the original data. In a new Fourier transform these sources have then disappeared together with their appropriate synthesized beam pattern.

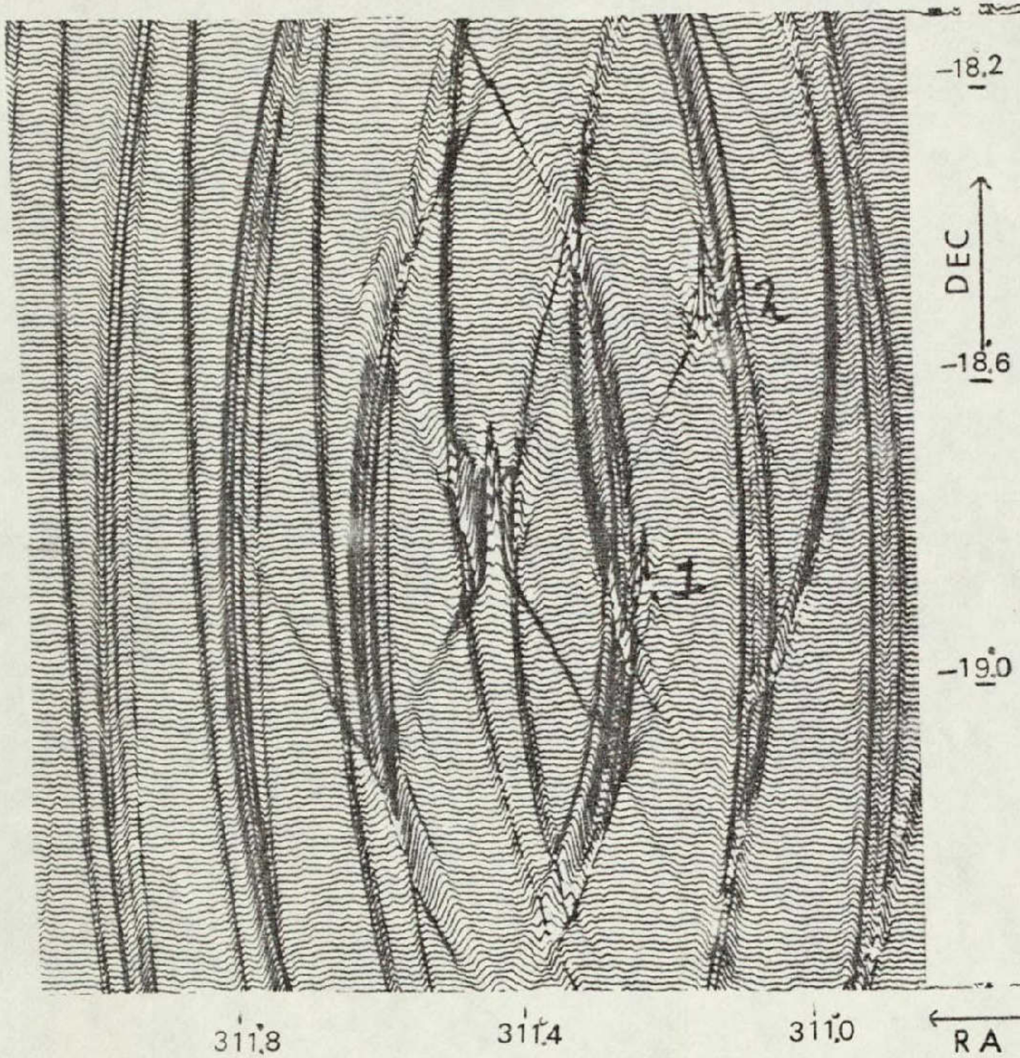

Fig.3.1. A "dirty" map of Jupiter at 21 cm.

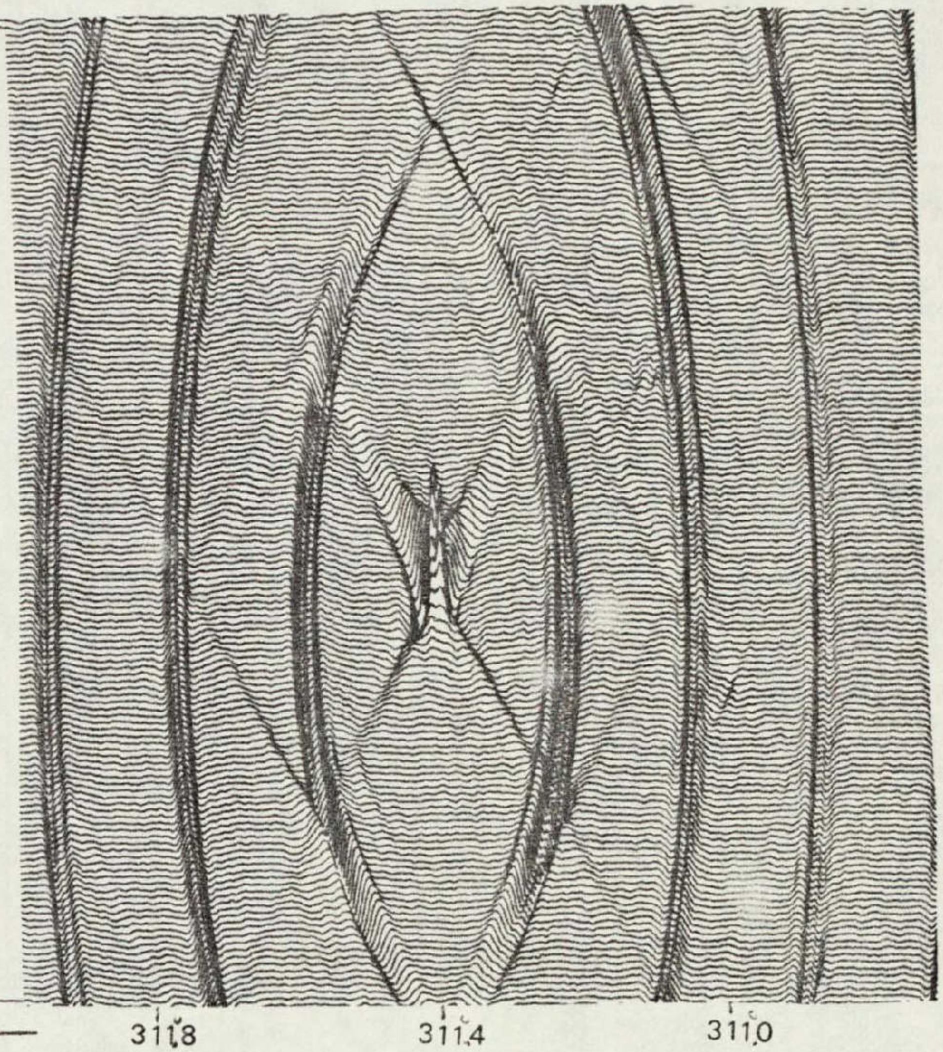

Fig.3.2. The background sources are subtracted now from the map of Fig.3.1

(This pattern is calculated as the response of the antenna to a point source at the position defined; it is assumed to be equal to the real pattern, see also Ch. III.3). The map after subtraction of these sources is shown in fig. 3.2. From the three observations we had at this wavelength we subtracted resp. 2, 5 and 6 background sources.

50 cm At this wavelength the field of view is much larger than at 21 cm and hence we expect much more troubles with background sources. To observe the planet radiation alone without the interference of background sources all fields were observed twice; the first time with the planet in the center of the field, during the second observation the planet was already far out the field of view. This second observation we subtract from the first one to obtain observations without any background sources.

6 cm During the measurements at this wavelength we had a lot of problems with the wheather and the stability of the system:

- the weather: there often was too strong a wind to be able to make observations at all; besides this there were a lot of snowshowers which influenced the total power output (or system temperature T_{syst}) in a way that it was increased irregularly by factors 10-12%. Knowing that the gain of the system

$$G(t,z) \sim \frac{1}{T_{syst}(t,z)}$$

it will be clear that the gain correction factors had to be increased in the same irregular way $T_{syst}(t,z)$ was increased. Moreover in this case we know that all total power variations were caused by atmospheric disturbances; thus the coëfficient P(Ch. II eq. 1) is now a time-dependent function P(t) and the gain factors had to be increased with an extra factor:

$$\frac{1+P(t).F(z)}{1+P.F(z)}$$

Both factors were determined with help of the total power chart records and the data were corrected for the snowshowers.

- the system: during a 7 hour measurement Jupiter is moving nearly 3' along the sky; this would (at 6 cm) give a significant attenuation of the radiation due to the primary beam of the individual antennas. We therefore decided to make a double-pointing during one measurement: before and after the meridian passage of the planet the telescopes should all be equally pointed to the mean positions of Jupiter during both half observing periods. In this way the amplitude variations would be less then 3 % (phases are not affected by the pointing of the telescopes). However the pointing of the (individual) telescopes turned out to be not very accurate at this wavelength for such low declinations. This fact we concluded from a discontinuous transition in amplitude, of about 10% at hour angle zero.

We tried to correct for this jump as well as was possible. The amplitude error left due to this effect I would estimate to be about 5 %.

We could not detect any background sources in the 6 cm maps of Jupiter after a fourier transformation was applied.

c. As was shown in fig. 3.2 we now can make maps of Jupiter but the planet is smeared due to both its motion and rotation. In order to get pictures at particular Jovian rotational aspects we have to remove both motions from our data (before a fourier transformation is done!)

1. removal of the planetary motion along the sky:

In chapter I the term "fringe stopping center" of an observation is explained. This center can be shifted to other coördinates after the observations have been completed which changes the phases of the datapoints. We even can apply a continuous time-dependent shift to this fringe stopping center and this is what we need to "stop" the planetary motion along the sky: when we let this center move in the way Jupiter has moved along the sky we change the phases of all data such that it looks like if the planet did not move at all.

This "trick" can be applied to the data with help of a special correction routine "planet" in REMOBS by defining $\Delta\alpha(t)$, a fourth order polynomial $\alpha_i t^i$ defined as:

$$\alpha_{true}(t) = \alpha_{obs} + \Delta\alpha\ (t) \qquad \text{where } \alpha_{true}\ (t)$$

represents the apparent time dependent coordinate of the source and α_{obs} the coördinate of the fringe stopping center.

With this routine we succesfully removed the planetary motions from the maps.

2. removal of the rotational motion:

To obtain pictures of Jupiter at particular rotational aspects one has to cut the 7 hour observations into small pieces in hour angle: the 6 and 21 cm data were clipped into 25^{min} pieces which is about 15 Jovian rotational degrees. At the radiation belts (lower frequencies) we expect than a smearing effect of 15", at the planetary surface (the main source of radiation at 6 cm) a smearing effect of about 5". The 50 cm data were only one-hour observations which corresponds to 36 Jovian rotational degrees and gives a smearing of 36". We expressed the longitudes belonging to each 25 min. piece in Syst. III (1965.0) coördinates (as described in Geoph. Res. Lett. (1977) 4, no. 2, p 65).

In the next section the method for obtaining one- and two-dimensional pictures of the planet from these short observations will be described.

3.2 Fourier transforming the data.

Using a computer program called MAKEMAP (see Internal Technical Report 79 of the NFRA) we can Fourier transform the data into brightness distributions of the sky (in all four Stokes parameters). To save computer time a Fas Fourier Transform algorithm (FFT, Cooley and Tuckey, 1965) is used for which the UV points are converted to a rectangular grid, equidistant in the U and V directions. The number of brightness points in the resultant map (rectangular matrix) is in integral powers of 2, not less than 8 and not larger than 512. This number can be chosen freely in both directions, together with the width of the map in RA and DEC. This width is often chosen such that there are (at least) 2 datapoints per half power beamwidth.
In the case of Jupiter we made a lot of observations on different days; since the planet was moving we got a variation in both the fluxes we received each day and the apparent sizes of the emission region due only to the variation in the distance Earth-Jupiter. To compensate for this effect we first multiplied all channels with a factor

$\frac{(E-J)^2}{4.04^2}$, where E-J represents the distance Earth-Jupiter in AU at the time the observation was made and 4.04 AU stands for the normalized E-J distance.

In order to facilitate the comparison between different frequencies we chose the width of the various maps in RA and DEC such that when all maps would be made at 50 cm the distances between two gridpoints were equal in each map when expressed in Jovian radii. By reducing the gridspacing for the 21 and 6 cm observations with factors of respectively 2 and 8 we were able to produce maps at all frequencies with the number of points per half power beamwidth between 2 and 2.5.

The short observations cover only a very small segment in the UV plane and hence have a resolution in mainly one direction, along the line through the source parallel to the projection of the Westerbork array.

At some Jovian longitudes we had more than one short observation, each with a different baseline orientation. Combining the datapoints we should get a better coverage of the U.V. plane and hence a better resolution in two dimensions. However since the apparent sizes of the emission region were varying from day to day due to the variation in the Earth-Jupiter distance we had to sample our maps as described above. We therefore had to Fourier transform all short observations separately and we could add the maps at the same rotational aspects of the planet afterwards. This basically gives the same result as Fourier transforming the combined UV points after the appropriate scaling.

In this way we could make maps at only a few Jovian longitudes (at 6 and 21cm) To obtain as much information as possible from the observations we therefore made also stripscans of the planet from all short observations at 21 and 50 cm. To obtain these scans, the datapoints of each short observation were added such that we got a pure one-dimensional distribution of the source along the line parallel to the projection of the Westerbork array.

Fig.3.3. a. A Jovian map at 21 cm constructed from three short observations at $l_{III}= 123^{o}$. The horizontal axis is the distance from the center of the planet in Jovian radii. The contour values in mJy/beam are: 25, 50, 100 - 1000 (in steps of 100) and similarly for the negative values; these contours are dotted. b. Pattern of the synthesized beam of the map in a. Contour values are: 0.05, 0.10, 0.20 - 1.0 (in steps of 0.20) and evenso for the negative values. These values have been chosen to more or less match Fig.a.
c. The "cleaned" Jovian map from a. The same contour values as in a are drawn. The planetary disk and the magnetic equator are indicated.

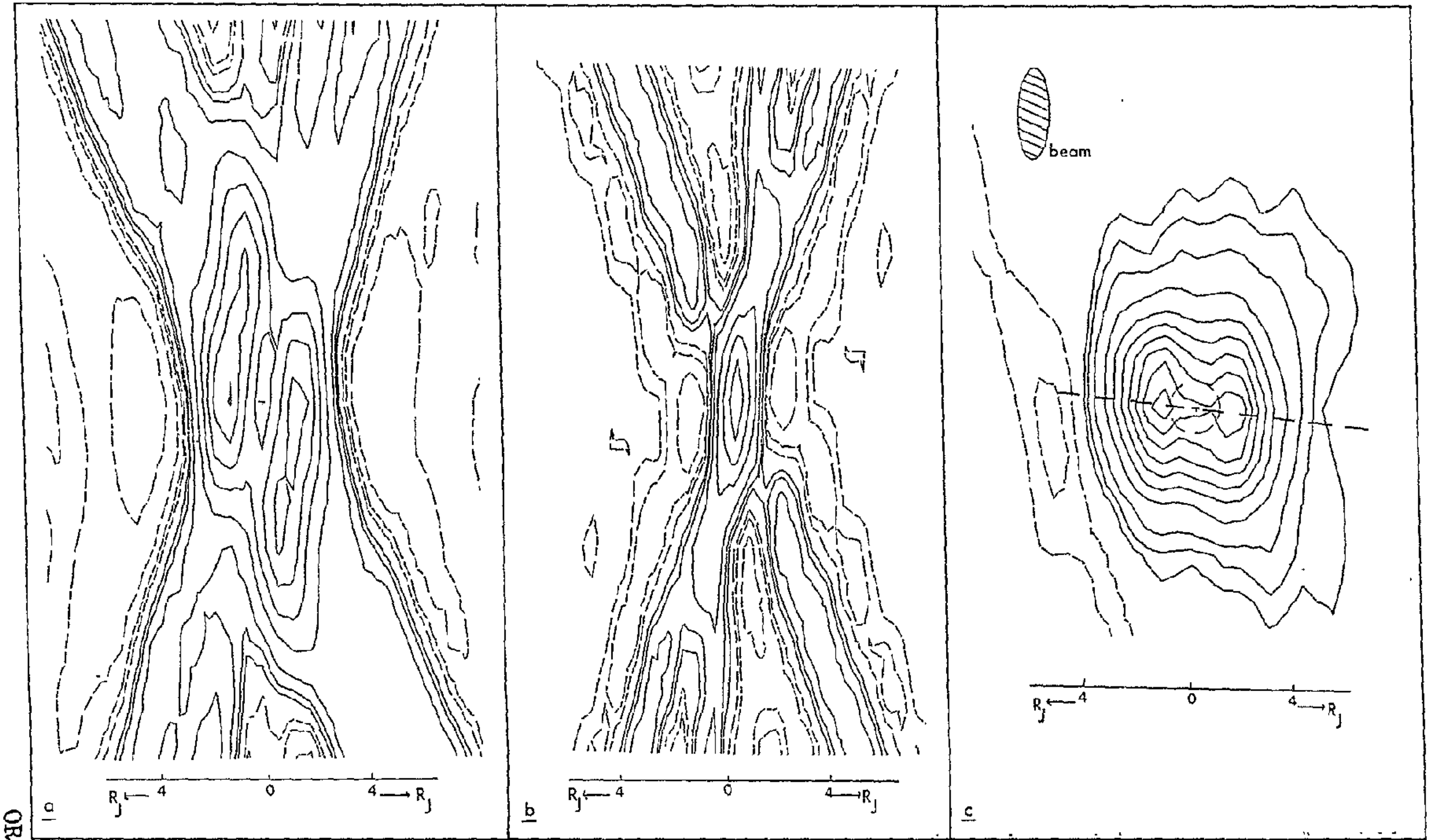

Fig.3.3

3.3 "Cleaning" technique.

In this section the "cleaning" or deconvolution technique we used is described (Högbom, 1974). Fig. 3.3a shows a map at 21 cm after fourier transforming and combining the data as described in the previous section. The expected grating responses are outside the picture and we see large distortions near the source due to the "dirty" beampattern of the telescope, shown in part b. (see Ch. II eq.3). We removed these effects with help of a procedure called "CLEAN", a deconvolution technique developed by Högbom (1974). As was already mentioned in Ch. III.1 the beampattern of the telescope can be "approximated"* by calculating the response of the antenna to a point source at the position of the original source and with the same aperture filling, taking due account of the grading function used. With help of these calculated beam patterns the WSRT maps are cleaned. As has already been said in the previous section, a map consists of a rectangular matrix filled with intensity values. "CLEAN" picks out the point with maximum intensity and removes a certain fraction of this flux from the map, as if it were a true point source at that gridpoint, thus removing with it the appropriate (calculated) beampattern. At the same time the position and intensity of the equivalent removed point is recorded on a new map. This procedure is repeated again and again until the original map is "empty" and the new map consists of the observed flux represented as a set of δ-functions with appropriate intensities at given gridpoint locations.

A realistic map is then restored by smoothing all the δ-components using an artificial beam (one without sidelobes) of the appropriate width. This beam in general is equal to the synthesized beampattern in between the

*When the observations are very good this calculated pattern is exactly the same as the real beam pattern; when there are calibrations or system stability problems both patterns do not fit entirely.

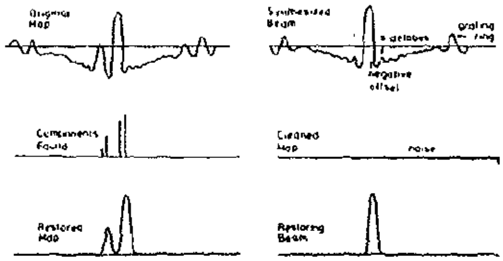

Fig.3.4. sketch of the procedure "CLEAN".

first zero's (see fig. 1.4) and equal to zero outside these points. Another possibility in the existing software is to take a Gaussian beam with a half power beamwidth about equal to the synthesized half power beam width. (Used with the Jupiter data since these did not cover a full UV plane). In the case of Jupiter we had to be careful in defining a certain region from which δ-components could be taken away otherwise the clean program would pick out flux components from regions where in reality no flux exists (i.e. from the ridges of the antenna pattern in the map). The result we got after having cleaned the map in fig. 3.3a is shown in part c. The negative ridge at the left hand side of the source and the shape of the outer contours are clearly due to the remnants of the true synthesized antennapattern of the telescope. The calculated beampattern does not fit the real pattern exactly as can be expected at such a low declination where the quality of the calibrations is always uncertain. (Ch. III.1).

Therefore the uncertainty in this map (and all others) is mainly due to this imperfect beam pattern. The negative ridge along the east side of Jupiter has a mean depth of about 35-40 mJy/beam which is the estimated uncertainty in this beam pattern. The system noise is only a few mJy/beam and the noise in the "cleaned" maps is 20-25 mJy/beam. Adding these quantities quadratically we find a total uncertainty of about 45 mJy/beam in all the 21 cm maps and stripscans. The uncertainty in the maps and stripscans of the polarized flux density is estimated in the same way as being 10-15 mJy/beam. The instrumental polarization is only 1-2 mJy/beam (Weiler, 1973). At 6 cm we have an additional error in the gain due to the instability of the system and the weather as was mentioned above. This error is about 5 % which is 60 mJy/beam for the maximum intensity. The noise due to amplitude and phase errors is 25-30 mJy/beam. The total uncertainty in these maps appears to be about 70 mJy/beam.

References

Bracewell. R., 1965: The Fourier transform and its applications. McGraw-Hill Book Company, New York.

Cooley, J.W. and Tuckey, J.W.B., 1965: Math. Comput. 19, 297.

Högbom, J.A., 1974: Astron. & Astrophys. Suppl. 15, 417.

Internal Technical Report ITR 79.

Weiler, K.W., 1973: Astron. & Astrophys. 26, 403.

Chapter IV. Results.

4.1. Integrated Jovian parameters.

Fig. 4.1 shows various parameters of the integrated Jovian radiation as functions of magnetic longitude (Syst. III 1965.0), averaged over 15° intervals (these quantities are calculated directly from the receiver output by extrapolating the baseline-dependence to zero baseline). Indicated are:

a) Polarization: The position angle of the electric vector measured eastward from the North of the sky. Because of the rotational pole of Jupiter was inclined from North by $342^{\circ}.7$ the mean position angle of the electric vector is centered around $76^{\circ}.7$ rather than around 90°.

b) Total integrated flux in Jy. In the extrapolation to zero baseline a gaussian shape of the source was assumed.

c) Degree of linear polarization.

d) Magnetic latitude of the earth with respect to Jupiter. This latitude Φ_m was calculated according to $\Phi_m = D_E + \beta \cos (l_{III} - l_0)$ (Berge and Gulkis, 1976). D_E is the declination of the earth relative to Jupiter's rotational equator (-0.29 at this epoch), β is the angle between Jupiter's magnetic and rotational axes taken as 10° and l_0 is the central meridian longitude of the magnetic Northpole taken as 201° (Syst. III 1965.0).

The variations with longitude are consistent with the beaming found by others from the integrated data (Berge and Gulkis, 1976; Gardner and Whiteoak, 1977; Neidehöfer e.a., 1977). Note the difference in flux-maxima and the deviation from a sine curve at longitudes larger than 200°. With help of a kind of a "hot spot" in Branson's maps (1968) near longitude 200°, Conway and Stannard (1972) suggest this spot to be responsible for the deviations from a sine curve in the pictures like Fig. 4.1. The existence of such a "hot spot" - I would rather call it a "hot region" - can now be proven with the maps and stripscans made with the Westerbork telescope in 1973 at 21 cm.

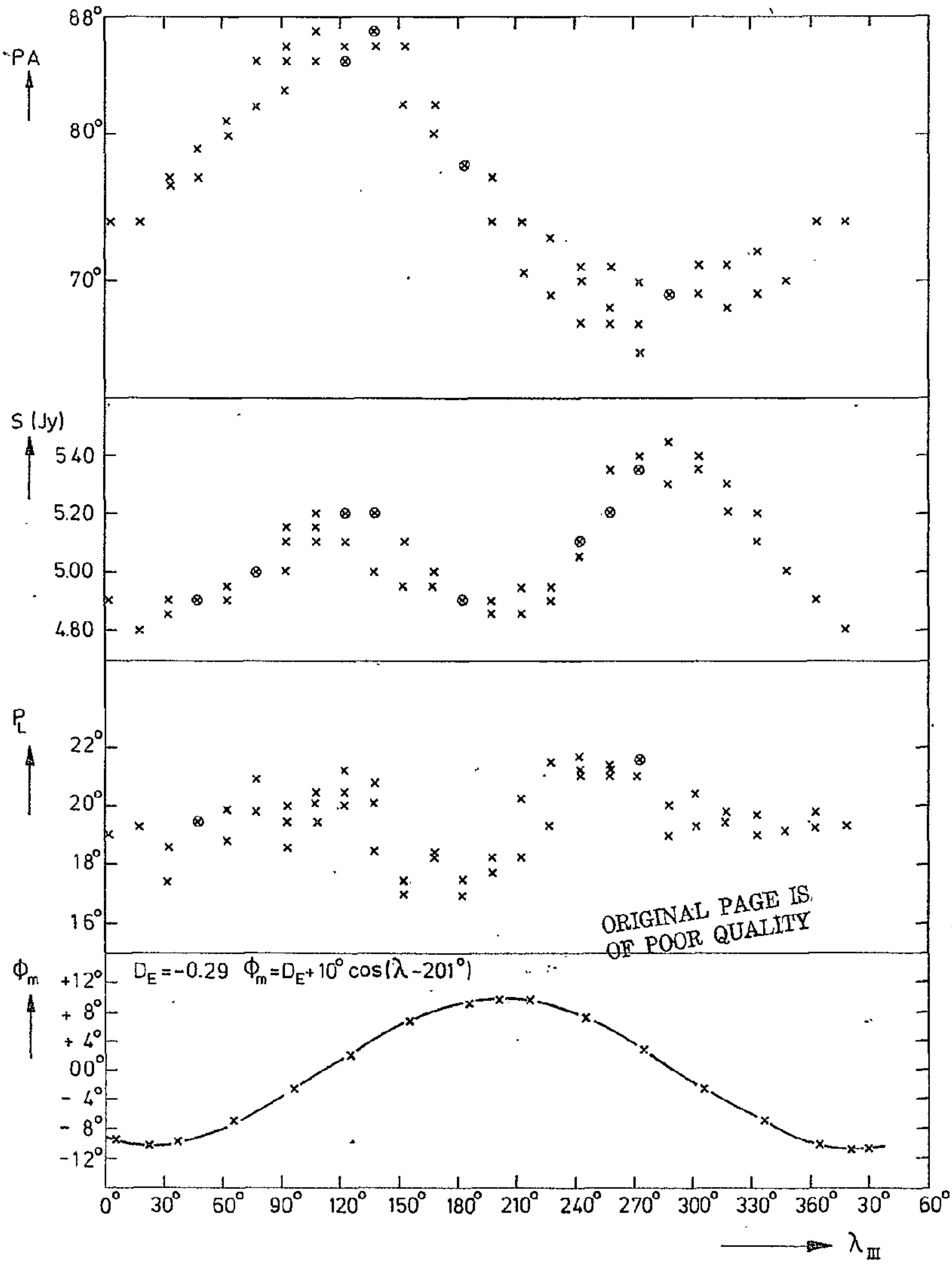

Fig. 4.1. Various parameters of the integrated radiation from Jupiter at 21 cm as functions of the magnetic longitude of Jupiter (in Syst. III. 1965.0).

a. Position angle of the electric vector measured eastward from North in the sky.

b. Total integrated flux in Jy.

c. Degree of linear polarization.

d. Magnetic latitude of the earth with respect to Jupiter.

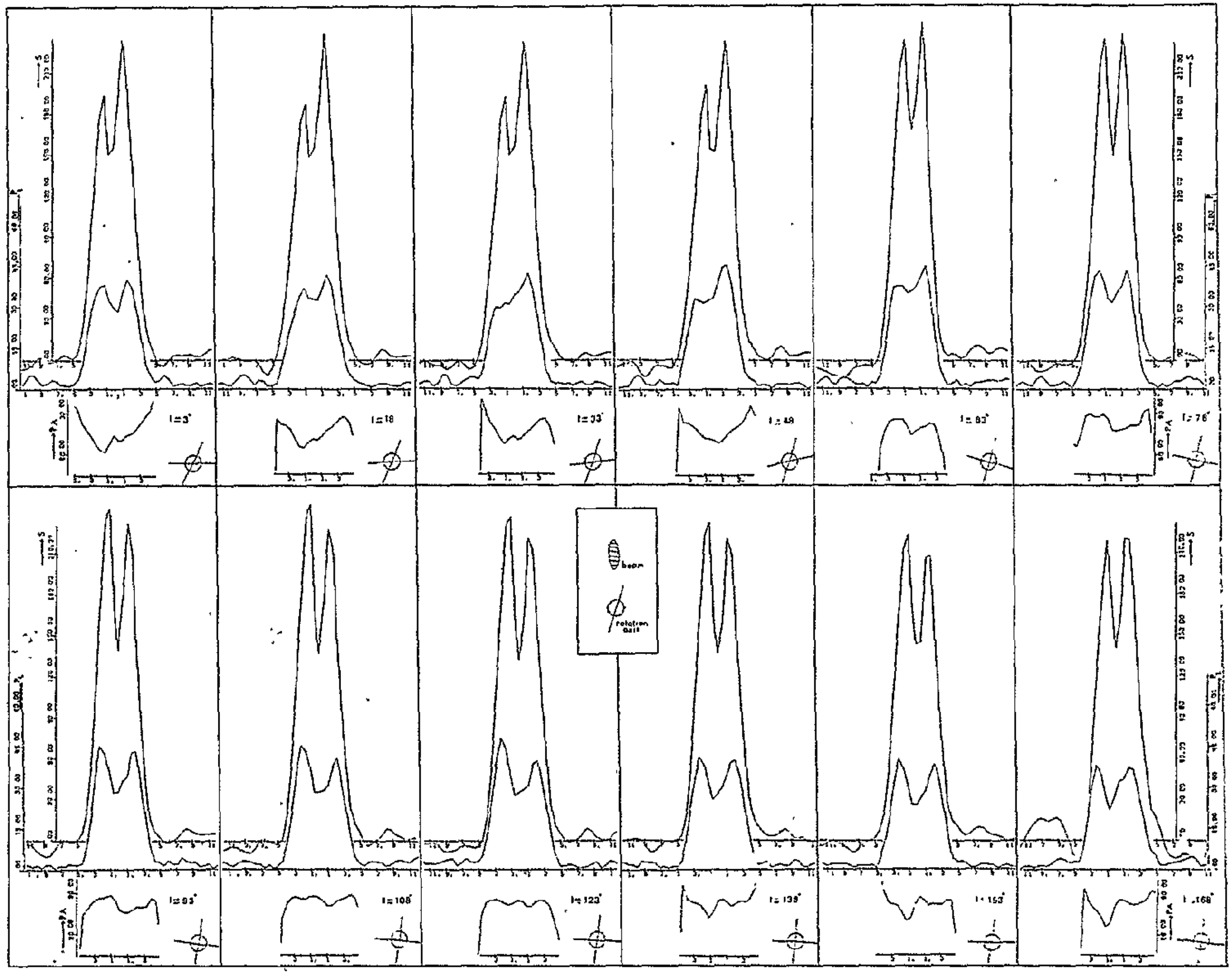

Fig.4.2 caption on page 29

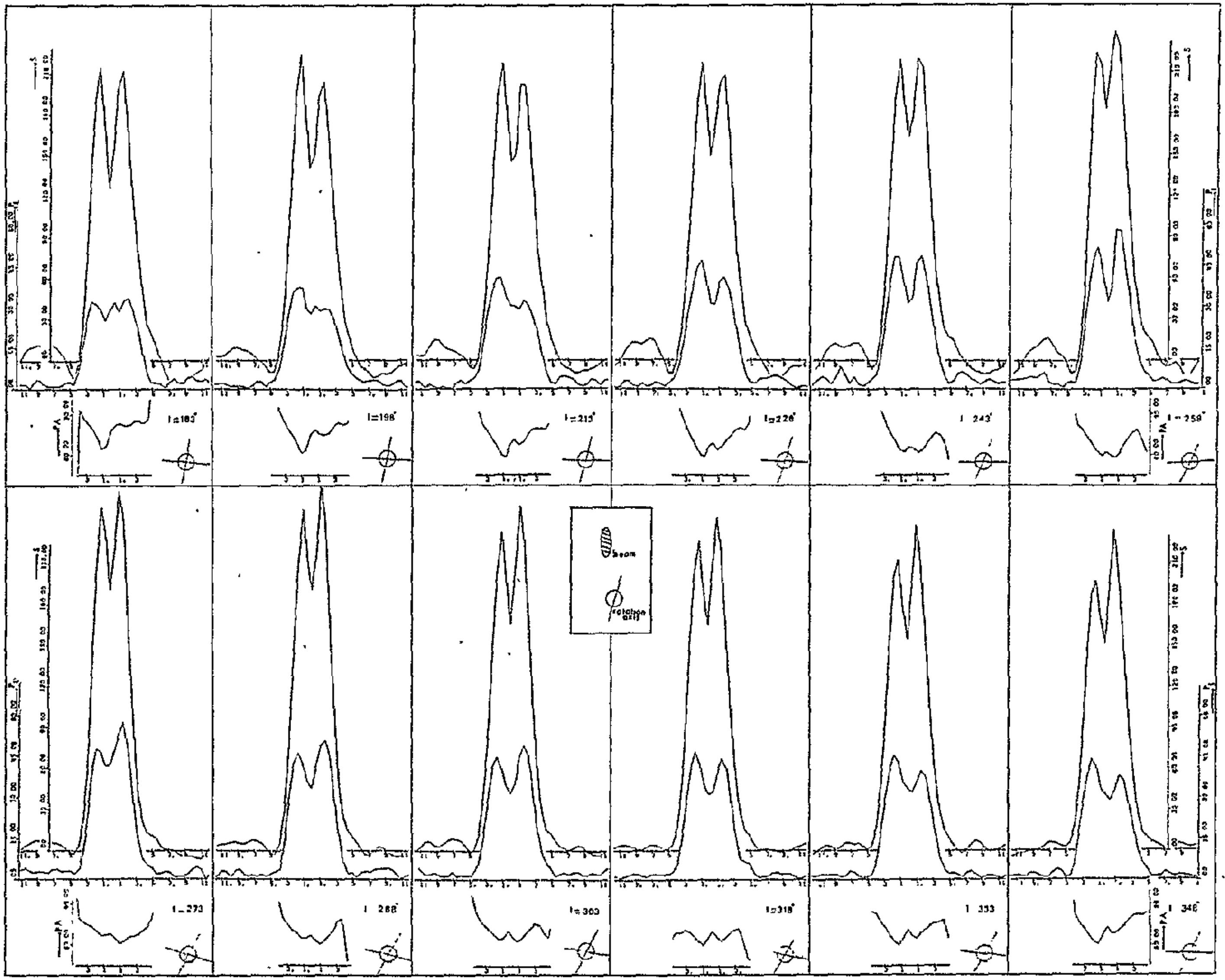

Fig.4.2 caption on page 29

4.2 One-dimensional stripscans

21 cm. Fig. 4.2 shows stripscans of the planet at 24 different rotation aspects (averaged over 15° Jovian rotational degrees). Indicated are the non thermal flux (with a model thermal flux subtracted, see below), linear polarized flux and position angle of the electric vector (see Fig. 4.1 for description). In the lower righthand corner of each plot the direction of the magnetic axis is indicated by the approximately vertical line and the direction along which the planet is resolved by the approximately horizontal line. In table I the exact values are given. Sometimes we had two or three stripscans at the same rotational aspect. Then we used the scan which was taken closest to the direction perpendicular to the magnetic axis which gives the best resolution without convolution due to the one-dimensional integration. The error in the scans I estimated as mentioned in section 3.3 to be about 45 mJy/beam in the non-thermal flux and 10 - 15 mJy/beam in the polarized flux density which gives ∿ 3° in the position angle. The fact that these angles have not been corrected for the Faraday rotation in the earth's ionosphere will result in an additional systematic error of less than 5° (Weiler and Raimond, 1976).

In these pictures as in all others the absolute position of the coordinate system is accurate to about 1". In Fig. 4.3 errorbars are indicated in the one-dimensional distributions at two different longitudes. The degree of linear polarization is sketched.

Fig. 4.2. Stripscans at 21 cm: each scan is averaged over 15° Jovian longitude Indicated are the non thermal flux, polarized flux ($\sqrt{Q^2+U^2}$) and the position angle of the electric vector. The fluxes are expressed in units of 5×10^{-29} W m^{-2} Hz^{-1} but they are convolved with the beam width. Since the maximum projected baseline length is different for each scan and also the spacing between two gridpoints is not equal this beamwidth is given in Table I for each longitude separately, relative to its mean value of 2.297. The horizontal axis is the distance from the center of the planet in Jovian radii. In the lower righthand corner of each plot the direction of the magnetic axis is indicated by the approximately vertical line and the direction along which the strip scan was taken by the approximately horizontal line.

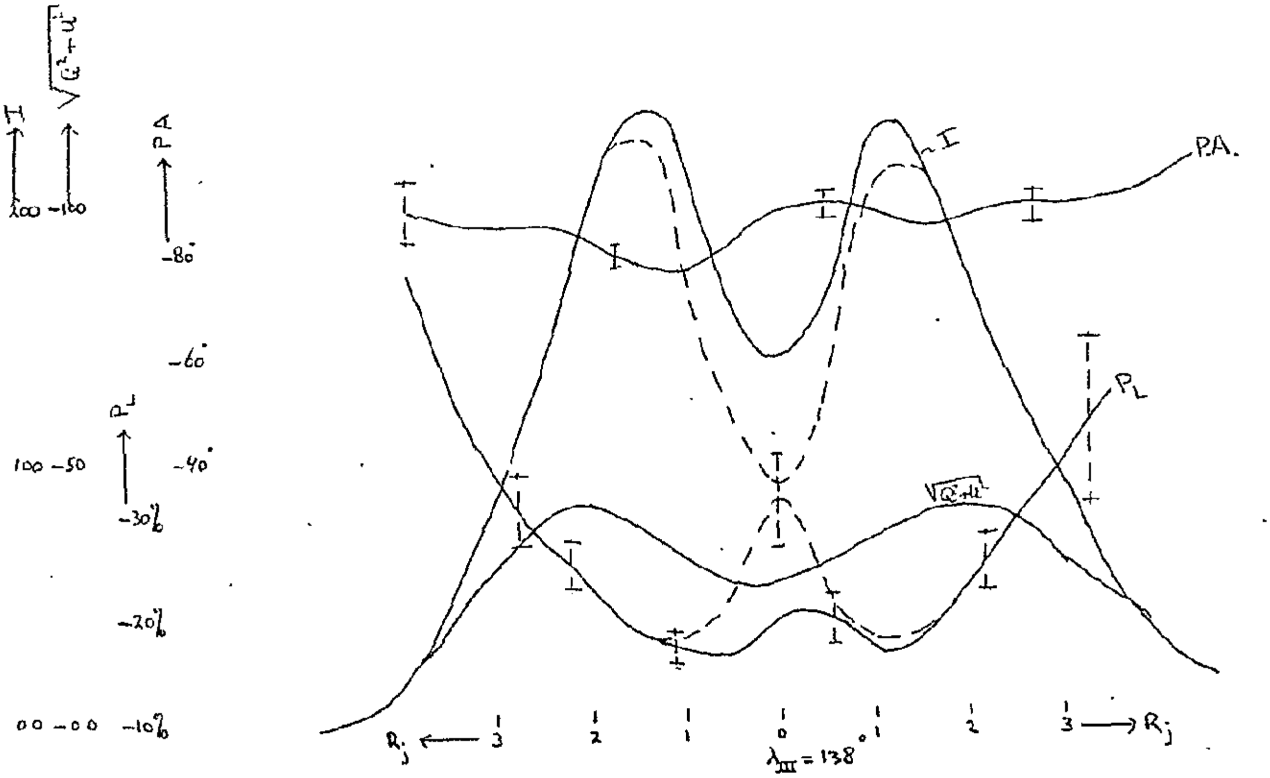

Fig. 4.3. The one-dimensional distributions of Fig. 4.2 and the linear polarization degree at λ_{III} = 138° and 273°. Indicated are error bars for each distribution. The non thermal flux was obtained by a subtraction of a 236 K disk (solid line) and a 387 K disk (dotted line).

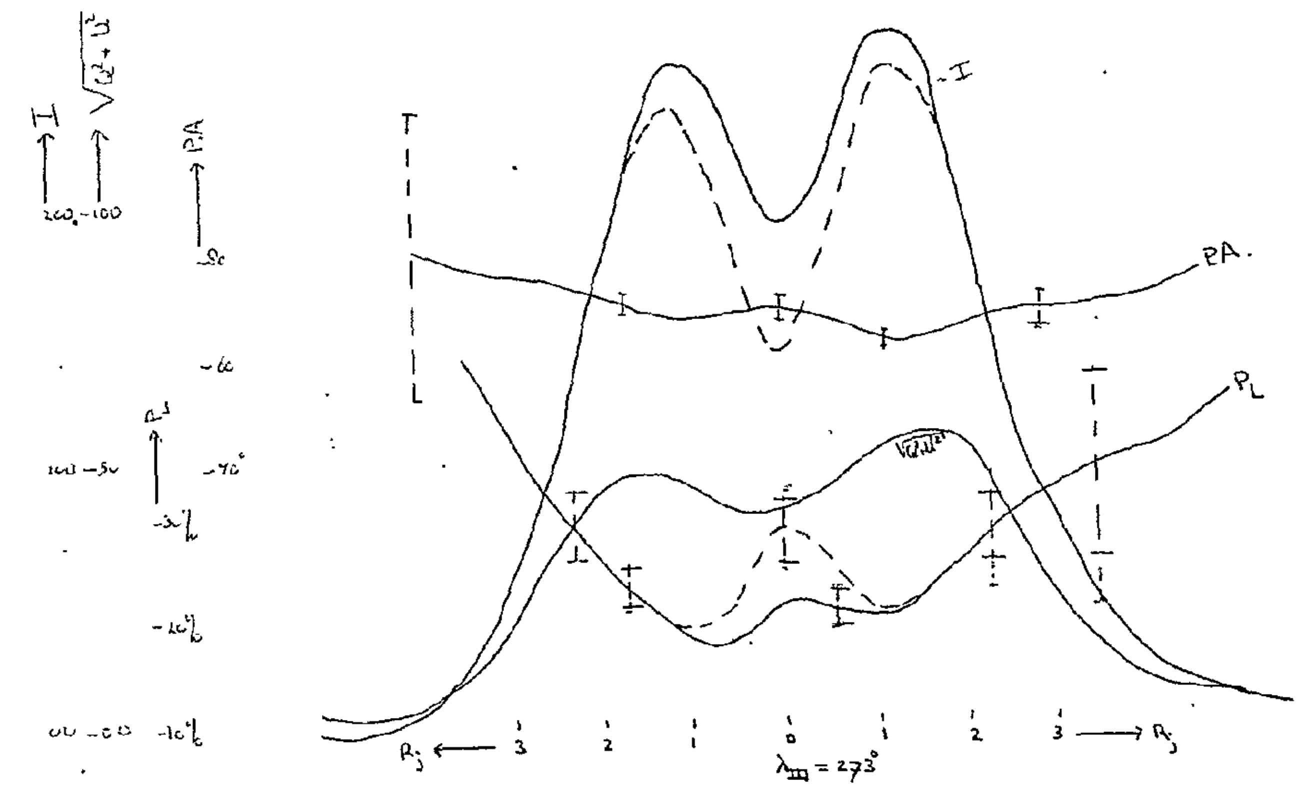

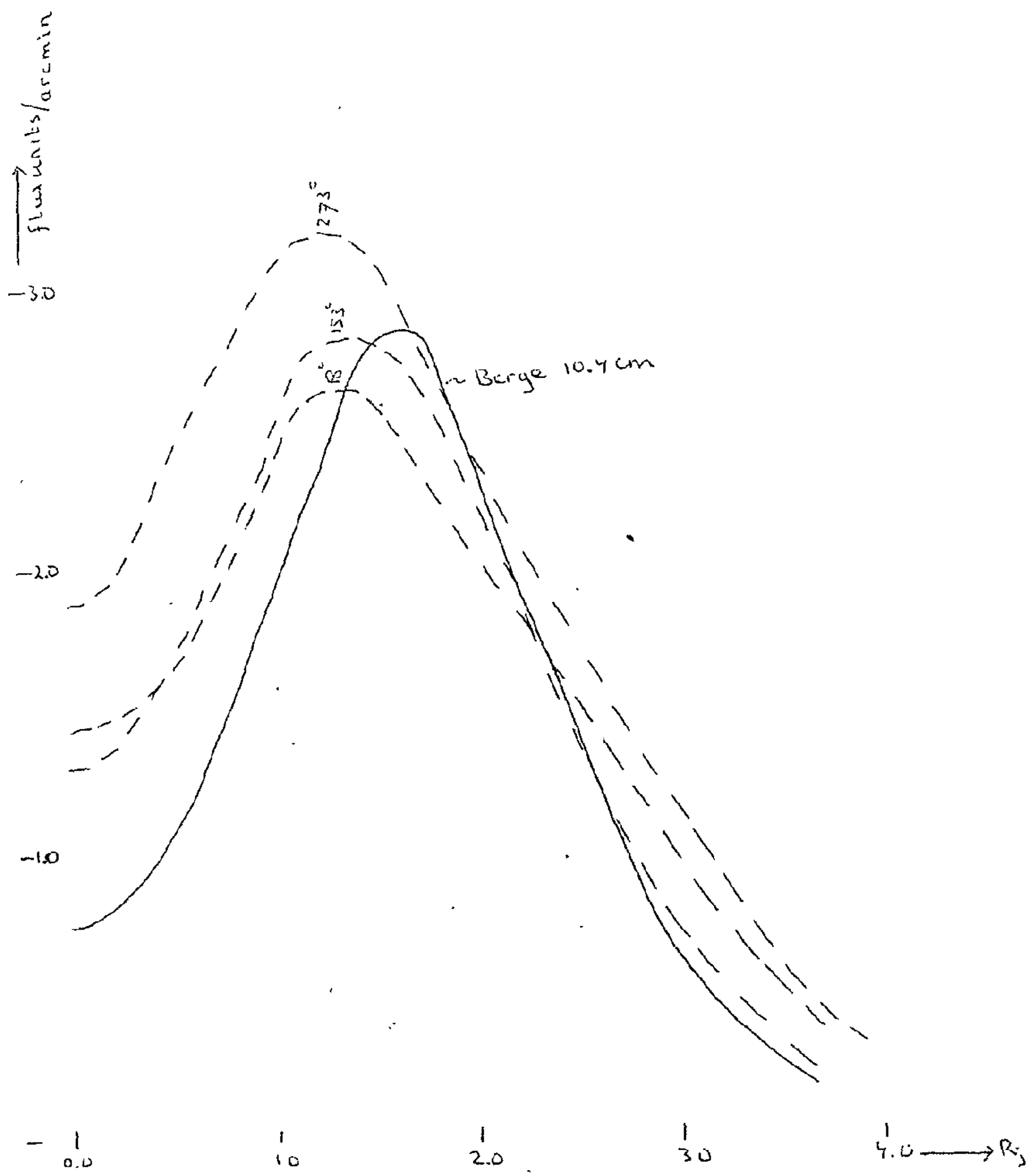

Fig. 4.4. Comparison of Berge's scan (Berge and Gulkis 1976) with some of our one-dimensional distributions. (with an assumed disktemperature of 387K).

Table I: Indicated are the position angle of the magnetic axis and the direction angle along which the stripscan was taken measured eastward from the North of the sky. The third column gives the sample spacing and the fourth the beamwidth relative to the mean value 2.297 gridpoints.

longitude in degrees	position angle of magnetic axis in degrees	direction angle of scan in degrees	beamwidth relative to 2.297 grid-points	sample spacing in arc sec.
3	339.4	269.9	0.999	9.911
18	340.3	271.9	0.999	9.911
33	344.9	273.9	0.999	9.911
48	347.5	276.0	0.999	9.911
63	349.8	256.5	1.004	9.888
78	351.7	259.3	1.004	9.888
93	352.8	261.7	1.003	9.888
108	353.3	264.0	1.003	9.888
123	353.0	266.1	1.002	9.888
138	352.1	268.1	1.002	9.888
153	350.6	270.1	1.001	9.888
168	348.5	263.4	0.999	9.934
183	346.0	265.6	0.998	9.934
198	343.2	267.6	0.998	9.934
213	340.4	269.7	0.997	9.934
228	337.8	271.7	0.997	9.934
243	335.5	273.7	0.997	9.934
258	333.8	275.8	0.996	9.934
273	332.6	256.2	1.002	9.911
288	332.2	259.0	1.002	9.911
303	332.3	261.4	1.001	9.911
318	333.2	263.7	1.001	9.911
333	334.8	265.7	1.000	9.911
348	336.9	267.9	1.000	9.911

The thermal disk temperature at 21 cm has never been defined properly by lack of good observations at this wavelenth and lack of understanding of the lower Jovian atmosphere.Estimated values for the temperature of the disk at 21 cm range from 236 K as found at 6 cm (see the next section) to ∿ 400 K as predicted by the theoretical curve of Gulkis (1973) for a convective model atmosphere with solar abundances of all chemical elements. The non-thermal stripscans in Fig.4.2 were obtained from the total flux density by a subtraction of a thermal disk of 236 K (modelled according to the footnote on page 40). Since the thermal disk temperature at this wavelenth is not well known as has been said before we also subtracted a thermal flux of ∿ 400 K in order to know to what extent the amount of thermal flux subtracted influences the shape of the radiation belts. The result is shown in Fig.4.3. It appears that the distances of the radiation peaks from the center of the disk do not change.

Fig.4.4 shows a comparison of some one-dimensional distributions with Berge's 10.4 cm scan (1966). Our scans here are made by folding over the East half on the West half and averaging it, after sutraction of a 387 K disk. Berge's scan I got by adding both polarized components (P.A. = 0^{o} and P.A. = 90^{o}) from fig. 3 in the article of Berge and Gulkis (1976). It is remarkable that the distance from the disk center to the flux.peaks is less in our scans than in Berge's scan by about 0.3 Rj. This shift resembles the shift as seen in Olsen's 3.7 cm and 11 cm data, plotted in fig. 4a, b in the same article. Remember the mean total flux of 5.1 Jy detected with Westerbork; Branson (1966) detected 6.6 Jy at the same wavelength, a value found by many others in that time (Table I, Berge and Gulkis 1976). Berge's 21 cm data from 1974 (fig. 5, same article) shows a mean flux of 5.1 - 5.2 Jy. All these data

are in agreementwith a sudden decrease in flux around 1972 (Klein, 1975; E.T.Olsen,1977: private communicatio). Possibly there is a relation btween this sudden decrease in flux and the inward shift of the radiation belt (E.T.Olsen,1977: private communication). Return to Fig.4.2. Since the resolution of the Westerbork telescope was about 2/3 of the disk diameter we really can distinguish both sides of the radiation belt. There is a clear difference in the amount of flux we receive from each side. (Note however also the angle between the magnetic axis and the direction along which the planet is resolved). From the variation with longitude I would estimate the existence of a hot region at a longitude of about $255^{o} \pm 10^{o}$. The whole series of scans also show the sinusoidal variation in flux, polarized flux and position angle as function of longitude. The width of the emission region profile also shows a small change corresponding to the hot region. It appears to be smallest at the longitude of the hot region and largest 90^{o} away from it. If we assume a ringlike structure for the radiation belt (see Fig.4.8) with an imbedded hot region the above data can be used to give rough estimates of the flux and size of this region. From the difference in fluxes received from both sides of the belt and the difference in the maxima of the total flux in fig. 4.1 I estimated the flux of the hot region to be about 0.4 Jy out of a total of about 4.5 Jy. With the additional information of the change in width of the emission region I estimated the extent to be about 50^{o} in longitude which means that its additional volume emissivity is enhanced by a factor of 1.6 with respect to the general radiation belts.
Branson's maps showed the hot region at a longitude of about 190^{o} (Syst. III 1965.0) and my data place it at 250^{o} - 260^{o}. Although Branson's maps are averaged over 120 Jovian rotational degrees an error of about 60^{o} seems rather large to me. Possibly this region moves or has moved through the belt. More observations are needed to clarify this problem.

50 cm. Fig. 4.5 shows the stripscans at 50 cm, obtained in the same way as the 21 cm scans. They are all made along the same direction which is indicated in the middle of the figure. In table II some physical parameters are written down, e.g. the total flux, which shows the same sinusoidal variation as the 21 cm data. As far as we can distinguish the two sides of the radiation belt the existence of a hot region at a longitude 250^{o} - 260^{o} is not in disagreement with these data. The error in the non thermal flux I would estimate to be about 45 mJy/beam according to section 3.3, in polarized flux 10 - 15 mJy/beam and hence a 2^{o} - 4^{o} error in the position angle of the electric vector.
The 50 cm scans are mainly useful in comparing the data at the three different wavelengths. This will be done in section 4 of this chapter.
In the next section the two-dimensional results at 6 cm and 21 cm will be described, together with a proper estimate of the thermal disk temperature at both wavelengths.

Table II: 50 cm data, see legend of Table I.

longitude in degrees	position angle of magnetic axis in degrees	direction angle of scan in degrees	beamwidth relative to 2.348	sample spacing in arc sec.	total flux in Jy
30	341.0	261.6	0.996	21.528	4.39
52	344.8		1.008	21.214	4.51
93	351.9		0.991	21.658	4.72
115	354.0		1.004	21.338	4.94
178	352.5		0.999	21.464	4.46
197	349.7		1.001	21.408	4.60
242	341.8		0.993	21.593	4.58
263	338.0		1.007	21.275	4.66

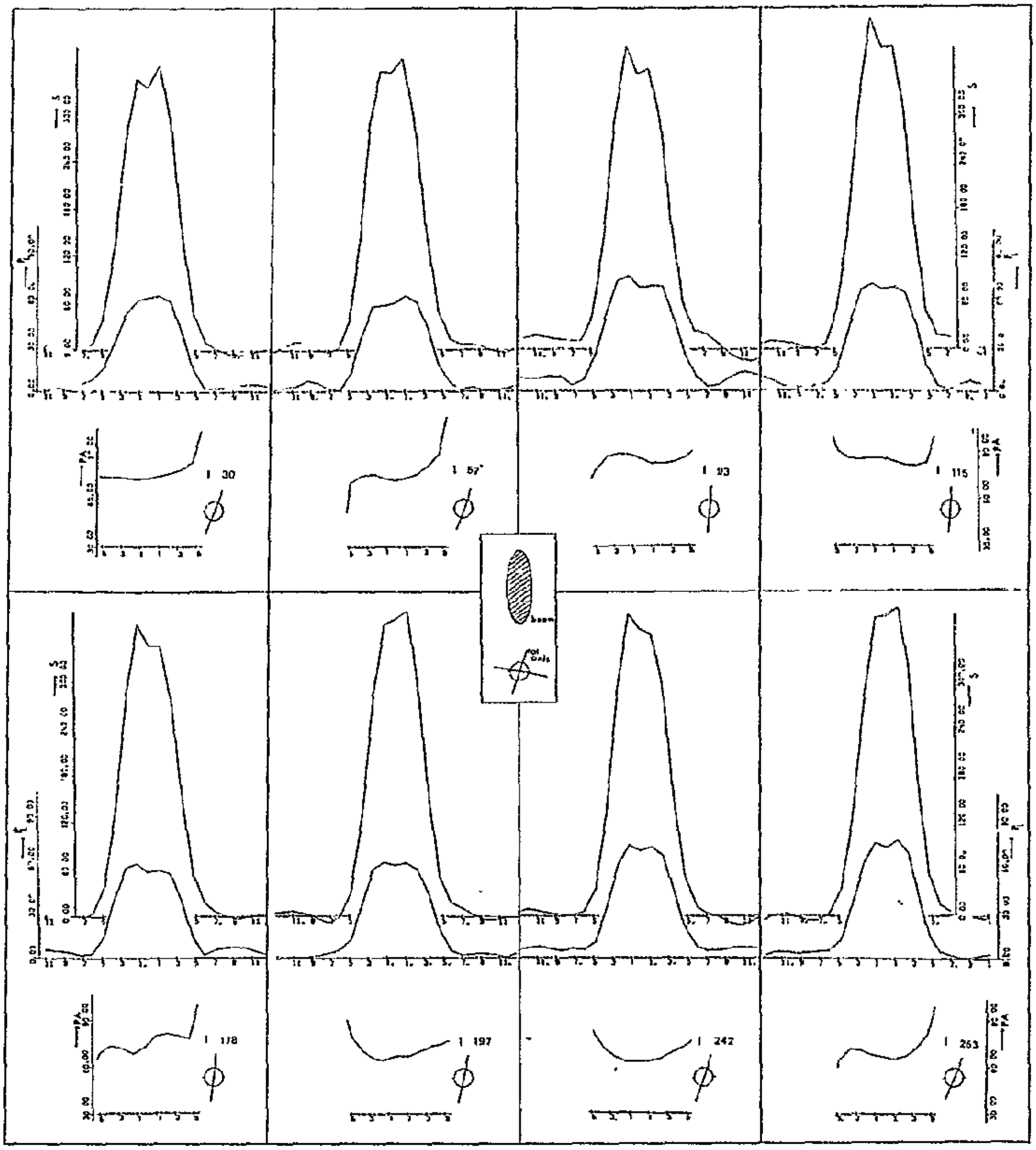

Fig. 4.5. Stripscans at a frequency of 0.6 GHz. See also caption of Fig. 4.2. In the middle of the figure the rotational axis is indicated together with the direction along which the source is resolved (by the approximately horizontal line).

4.3 Two dimensional Jovian pictures.

6 cm Fig. 4.6 shows two of the 6 cm maps we produced. Due to a combination of the low declination and the bad weather and system behaviour (Ch.III.1) the results at this wavelength were a little disappointing. We got five reasonable maps. Two of them are constructed from six short observations, the three other maps from five observations. The longitude in map a is indicated in syst. III (1965), in map b in Syst. I.

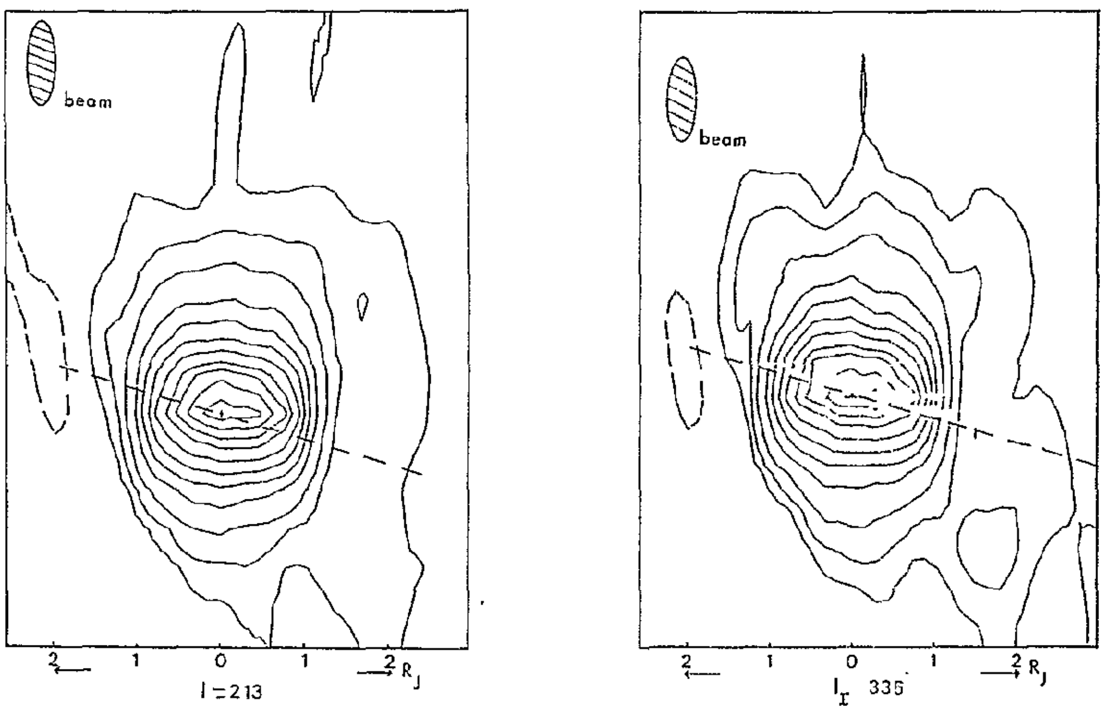

Fig. 4.6 Maps of the total intensity at 6 cm.

a. at a longitude $\lambda_{III}(1965) = 213^{\circ}$

b. at a longitude $\lambda_{I} = 335^{\circ}$.

Contour values in mJy/beam: 35, 75, 150 - 900 (in steps of 150), 1000, 1100, 1200, -35, -75. The negative contours are dotted; the beam width is 6.2980 gridpoints.

All five maps show the planet clearly resolved in the E.W. direction and they are quite similar in appearance. This probably means that there are no longitude dependent features on the disk with a deviation in intensity more than about 8 % of the maximum, a value which is estimated from the 70 mJy/beam uncertainty in the maps. The apparent strong decrease in intensity from the center to the limb in the declination direction is probably not real. The weather was so bad during the period of the 6 cm observations it is likely that the atmospheric extinction was larger than generally assumed. With the synthesis interferometer, the data giving the north-south discrimination in the source were obtained when Jupiter was near the horizon at large hour angles where the extinction correction was most serious. We therefore expect the polar intensities to be lower than they ought to be.

The fact that we do not see the radiation belts outside the thermal emission region is probably due to the rather high noise level.Assuming a flat spectrum for the non-thermal radiation we expect to detect a flux density of not more than 90 mJy/beam at the peaks of the radiation belts which is just one standard deviation. After convolution to the resolution of a 21-cm or 50-cm beam the whole emission region shows up.

Fig.4.7 shows a cut through the planet in the E.W. direction after subtraction of non-thermal radiation approximated by a model with a peak intensity of 90 mJy/beam at a distance larger than 1.4 R_J and decreasing to 36 mJy/beam in front of the planet. This model then was convolved with the proper beam. As a comparison we modelled the thermal emission of the planet by a uniform oblate disk filled

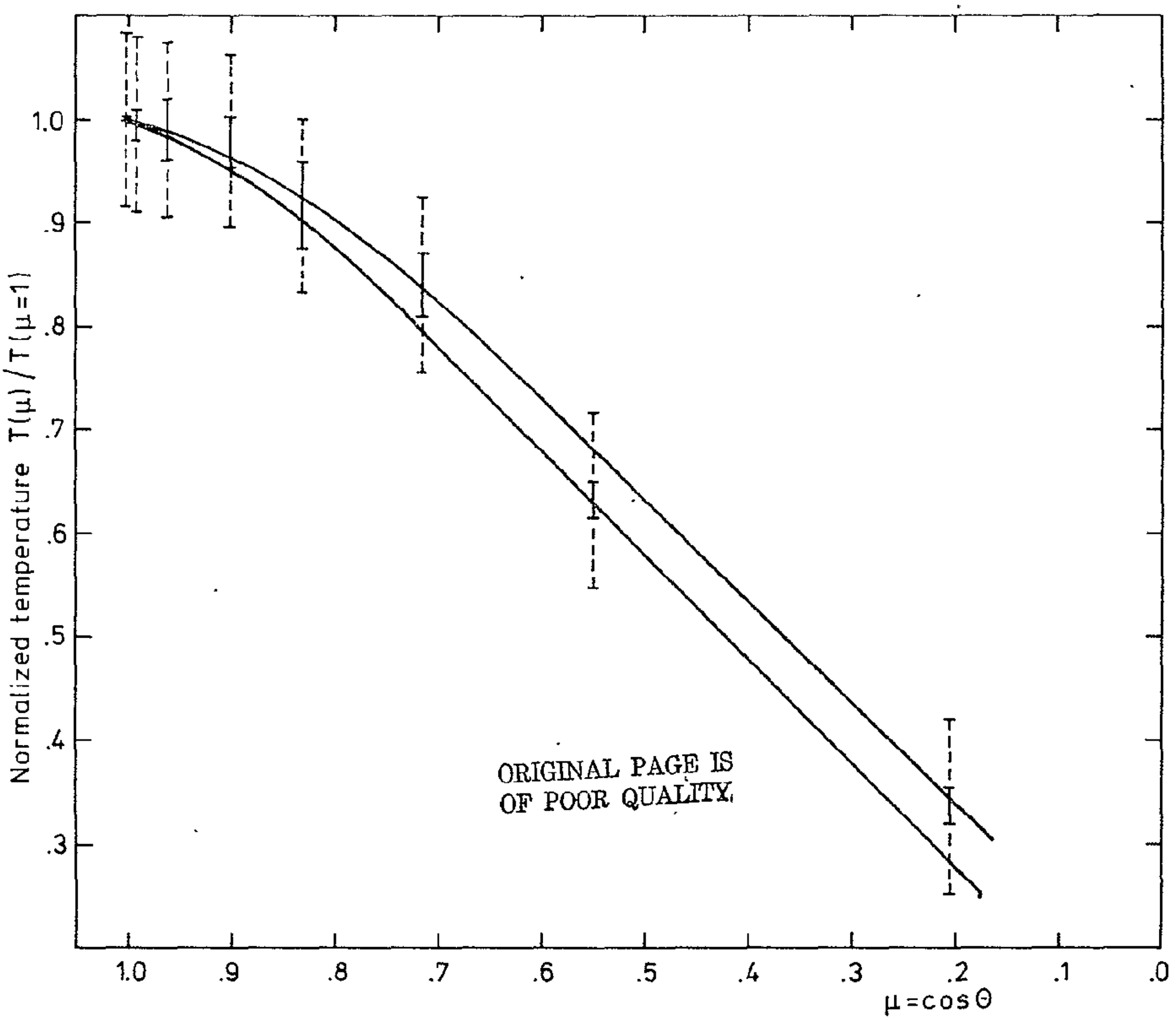

Fig. 7. A cut through the planet at 6 cm. The parameter $\mu = \cos\theta$ is indicated on the horizontal axis. θ is the angle a ray makes with the vertical to the atmosphere. On the vertical axis the normalized temperature $T(\mu)/T(\mu = 1)$ is indicated. The two curves drawn represent models of the oblate disk with (the lower curve) and without (upper curve) limb darkening (according to Berge and Gulkis, 1976) taken into account. For more details the reader is referred to the text. The vertical solid lines indicate the range of temperatures shown by the five Westerbork maps, the dotted lines are a measure of the error in each of these maps; they are drawn starting at the middle of the solid lines.

with volume elements of 2".5 x 2".5 and the disk was then convolved with the proper beam. The upper curve in Figure 7 shows the predicted temperature curve in the E.W. direction. Then the disk was limb darkened according to the theoretical curve of Berge and Gulkis (1976) for an ammonia mixing ratio in Jupiter's atmosphere of 1.5×10^{-4} and convolved with the beam to give the lower curve in Figure 7. An increase in the ammonia mixing ratio will reduce the apparent limb darkening moving the curve closer to that of the non limb darkened case. As was to be expected the measurements are rather insensitive to limb darkening but there is a slight tendency toward less limb darkening than expected from the curve of Berge and Gulkis (1976).

The thermal disk temperature at 6 cm was estimated from all five maps to be 236 ± 15 K which corresponds to a flux of 7.4 ± 0.4 Jy. The quoted error is that of any individual map. The temperature was determined simply by integrating the flux inside the 75 mJy/beam contour and subtracting from it an estimated non-thermal contribution equal to 60 mJy/beam outside the visible disk and one-half of this amount in front of the disk.

<u>21 cm</u> Fig. 3. 3 already showed a two dimensional picture of Jupiter at 21 cm. At seven different rotation aspects of the planet we had enough observational information to construct these kind of maps. The radiation shown however is the total radiation received from the planet. Before we can make pictures of only the nonthermal radiation we have to make a proper separation between the thermal and the nonthermal components of the emission. Taking the theoretical curve of Gulkis (1973) for a convective model atmosphere with solar abundances of all chemical elements the temperature of the Jovian disk

would be about 400 K. Assuming a blackbody radiation the temperature would be equal to 236 K, the value found at 6 cm.

To determine an accurate temperature at this wavelength we compared the observed variation of both the total intensity and the degree of linear polarization across the equatorial plane of Jupiter with values calculated for different models. The total intensity of the radiation belts was modelled by a series of uniform isotropic cylinders circling the planet as shown in the top view in Fig. 8a with the dimensions shown in Fig. 8b. The integrated brightness along the line of sight at the peaks of the radiation belts and at the center of the disk were then evaluated and compared with the observed values after subtraction of disks* with various brightness temperatures. The line of sight integrals of the volume emissivities V_1 and V_2 were calculated according to the method of Beard and Luthey (1973). An isotropic distribution of particles in the belts was assumed. The ratio V_2/V_1 is not more than 3.5 which after convolution with the proper beam leaves a factor of about 2.5. A more realistic model with a tapered distribution of particles (according to Beard and Luthey's (1973) model) would lower the ratio even more.

The observed volume emissivity V_1 along the equator in Fig. 8b after subtraction of a thermal disk of 387 K is about zero and the ratios V_2/V_1 come out to be 6.3 for a subtracted disk of 315 K, 5 for 300 K and 3.5 for 236 K. These maps however indicate considerable emission over the pole of Jupiter, which is difficult to understand in comparison with previous observations (Roberts, 1976) and which may be caused

ORIGINAL PAGE IS OF POOR QUALITY

* We modelled the oblate disk by filling it with volume elements of 2".5x2".5 and taking into account Olsen's limb darkening curve at this wavelength (private communication). This than was convolved with the proper beam. The limb darkening gives only a slight change with respect to a disk model where only the surface of the disk is taken into account.

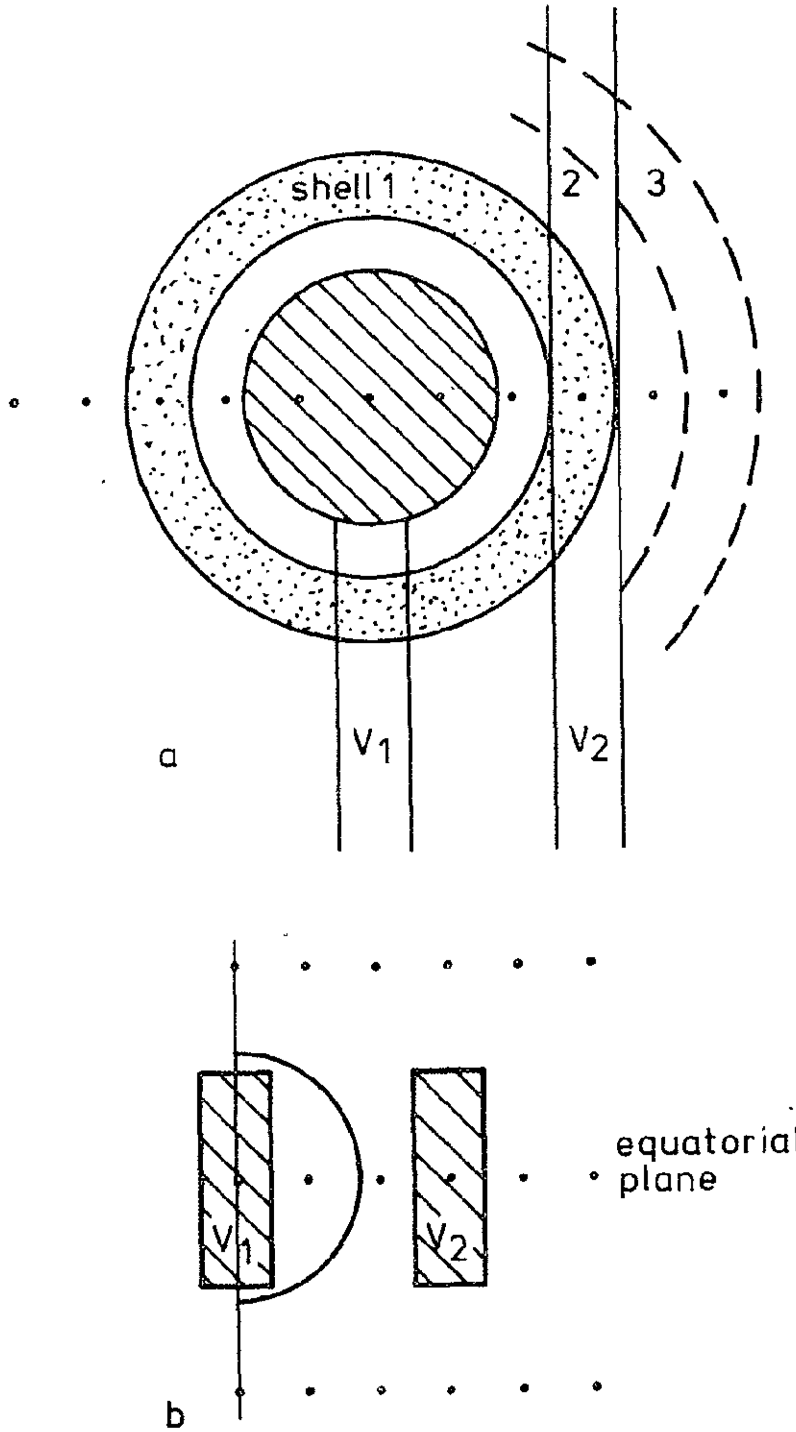

Fig.4.8. a. Top view of the model of Jupiter's radiation belts.

b. Observer's view of the model of Jupiter's radiation belts. The dots represent its matrix of datapoints on the Westerbork map at 21 cm with the size of the Jovian disk indicated by the thick line. The belts are modelled by three cylindrical shells as indicated in a. Each shell has a hickness of 1 gridpoint. Integration over the rectangles V_1 and V_2 along the line of sight gives the volume emissivity at the gridpoint in the center.

(in part) by uncertainties in the beam pattern due to phase errors in the measurements. The r.m.s. phase errors in the Jovian data can be interpreted as positional errors of $\sim 1''.5$. Since the maps are costructed with only three very small segments in the UV plane being filled this error will be amplified by a factor of $\sim$ 7 in the declination direction due to the small anglesbetween the projected baselines. In that case a decrease in flux density at the center of the disk of $\sim$ 7% can be expected; this decrease will be removed toward the poles. Taking into account all possible errors in the data the ratio between the volume emissivities V_2/V_1 can be decreased to $\sim$ 3 with a 300 K disk subtracted. Assuming the extreme case that no radiation at all comes from over the poles we can compare the integrated center-to-limb radiation of the stripscans seen in Fig.3 and 4. Here a ratio V_2/V_1 of 2.5 gives a disk temperature of 360 K.

Fig.9 shows the degree of linear polarization in the equatorial plane of the two- dimensional maps after subtraction of thermal disk models of various temperatures. With an expected increase in the degree of linear polarization just in front of the planet we estimated a lower limit of 270 K for the disk temperature. The various temperatures defined above were all estimated from maps where we see the magnetic equator roughly edge-on and the hot region is more or less behind the planet. All the above considerations lead us to adopt a mean disk temperature for Jupiter at 21 cm of about 300 - 320 K.

The fact that this temperature is perhaps 80 K lower than Gulkis' value can most easily interpreted as being due to a larger mixing ratio of ammonia as suggested by Tomasko, Dickel and Goodman (1974) to match Branson's (1968) published disk temperature and models of the radiation belts by Degioanni (1973). Other possibilities looked for were changes in atmospheric structure caused by the existence of a large amount of water or a strong absorption by NH_4SH.

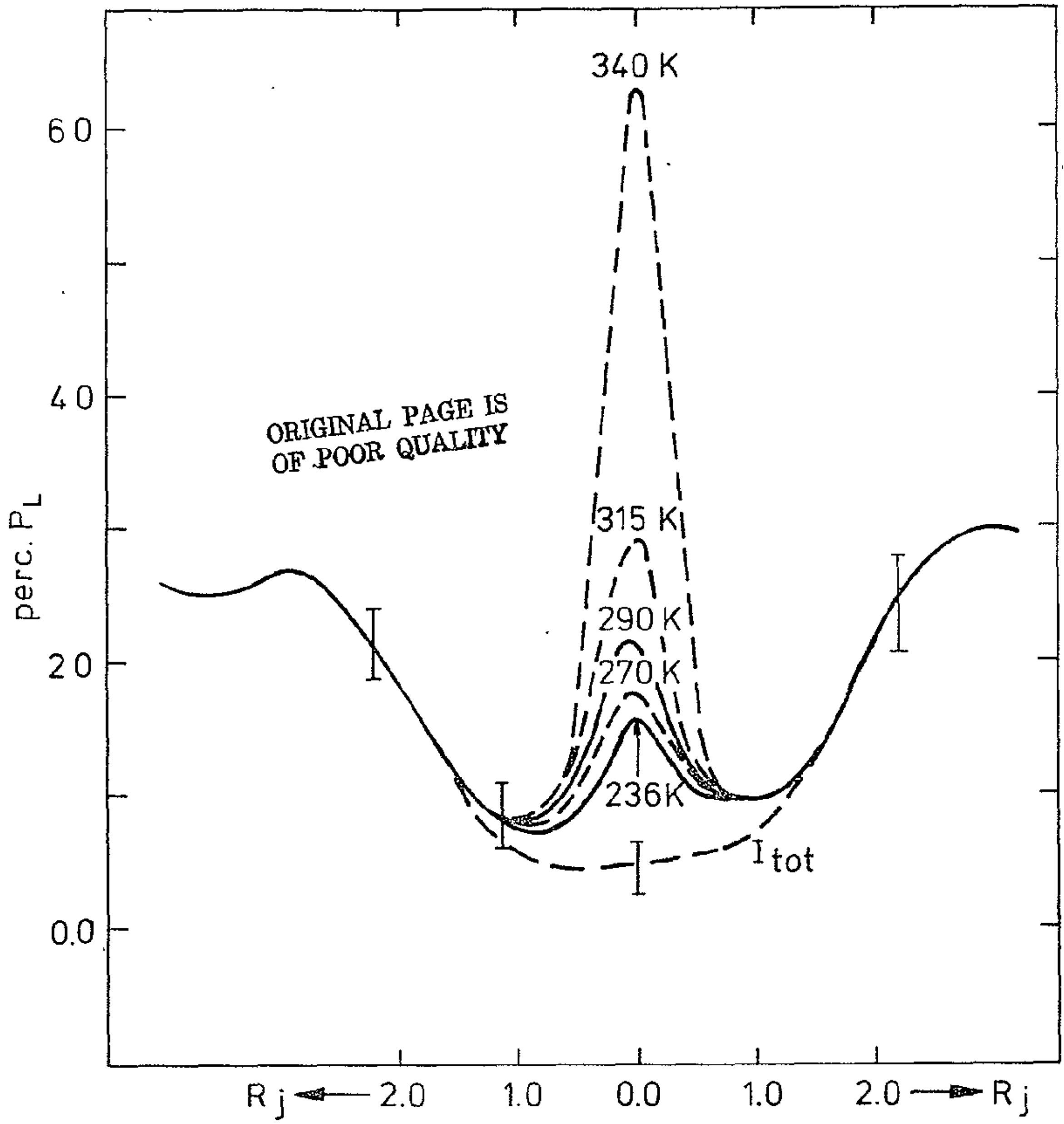

Fig.4.9. The degree of linear polarization in the equatorial plane at 21 cm. The lowest curve gives this degree for the total radiation received from the planet. The other curves show it for various disks subtracted: 236 K, 270 K, 290 K, 315 K and 340 K. A few errorbars are indicated.

The existence of a kind of a physical (solid) surface near 270 K is a very unrealistic model as was pointed out by Goodman (1969). Based upon the detection of a very small amount of watervapor at 5 μ (Larson et al. 1975) smaller than would be expected from the vapor pressure of water at 230 K, the temperature of the Jovian disk at 5 μ, one can point out that the mixing ratio of water certainly is less than ∿ 10^{-5}. To raise the mixing ratio of water would require sinks of water ice or droplets in which case an aqueous ammonia solution should exist (assuming a uniform distribution of the droplets or waterice) so that the mixing ratio of ammonia would need to become ∿ 10^3 times the solar ratio which is much too high for the observations at shorter radio wavelengths. Based upon the same kind of arguments we do not expect a noticeable absorption by NH_4SH (Lewis, 1969). The only way left (assuming a uniformly mixed atmosphere) to decrease the Jovian temperature to our measured value is to increase the ammonia mixing ratio by a factor of 4 to 5 with respect to the solar value of 1.5×10^{-4}. This is about equal to the factor by which Wallace and Hunten (1977) increased their mixing ratio of CH_4 in the region 0.4 - 1.1 μ. Together with the depletion of oxygen by a factor > 100 compared with the solar value these abundances will be very interesting for future work.

The maps of the non-thermal emission of Jupiter after subtraction of a thermal disk model of 290 K are shown in figure 10. The uncertainty in the maps is ∿ 45 mJy/beam as has been said in section 2. The southward shift of the radiation belts seen in the lower three pictures is probably not real, but due to a positional error in one or more of the three short observations as has been explained in the discussion concerning the definement of a thermal disk temperature. Squeezing the plotscale from Fig. 10 in declination by a factor sin δ relative to the scale in right ascension will give the appearance of the maps having been made with a circular beam. Any non-circularity then is due to a true exten of the radiating region in that direction. According to Berge's (1966) model we would expect an extent in declination of about 30" for the radiation belts (at the half power level). With a beam extent of ∿ 70" in

that direction we do not expect to resolve the belts in the N-S direction Fig. 11 shows the result for $\lambda_{III} = 108^0$. Part a is the total radiation map, b-f are the maps with a thermal disk of 236 K, 270 K, 290 K, 315 K

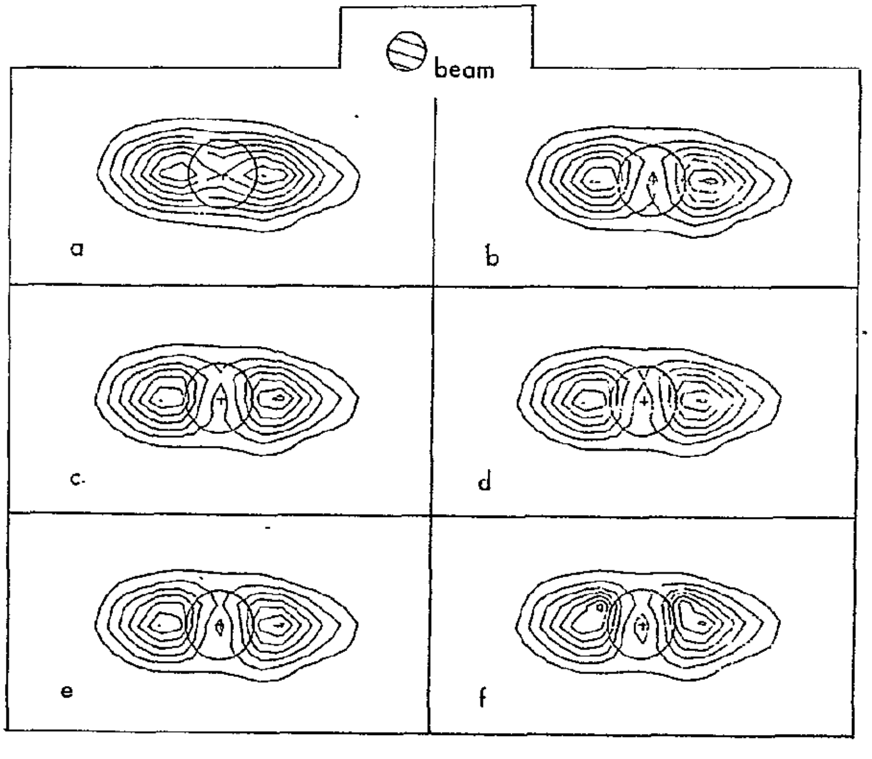

Fig. 11. Maps of the Jovian radiation with the plotscale decreased with a factor sinδ . λ_{III}=108 at 21cm.

a. total radiation, b-f the emission with subtracted a thermal disk of 236K, 270K, 290K, 315K, and 340K respectively.

Note that the planetary disk indicated in fact also had to be decreased with a factor sinδ in declination.

and 340 K respectively subtracted. There is clearly an extension of the belts in the right ascension direction in agreement with Berge's model. The pictures b-e also show that there is only a slight difference between subtraction of a thermal disk of 236 K or of 315 K. Here again as in the stripscans the distance between the peaks of the belts is smaller than in Berge's model.

Fig. 12 shows the polarized flux density $\sqrt{Q^2+U^2}$ and Figure 13 the position angles of the electric vector superimposed on the intensity maps of Fig. 10. The length of these vectors is a measure of the intensity of the polarized flux. These angles all appear reasonably parallel on the two sides of the planet. To get information on the magnitude of any magnetic anomaly associated with the hot region we need more sensitive data.

Fig. 10. Maps of the non-thermal emission at 21 cm from Jupiter's radiation belts. A thermal disk of 290 K has been subtracted from the total radiation received. Contour values in mJy/beam : 150-1050 in steps of 100. The beam area is 4.9868 points. The gridpoint spacing is 9".888 (= 0.55 R_j) in RA and 30".869 in DEC. The various longitudes are indicated in Syst. III (1965.0). The magnetic equator and the planetary disk are sketched in the pictures by dotted lines. On the horizontal axis is the distance from the center of the planet in Jovian radii.

Fig. 12. Polarized flux density $\sqrt{Q^2+U^2}$ of the maps in Fig. 10. Contour values in mJy/beam: 35 - 200 in steps of 15.

Fig. 13. Position angles of the electric vectors at 21 cm superimposed on the intensity maps from Fig. 10. The angles are measured eastward from the north in the sky. The length of these vectors is a measure of the intensity of the polarized flux from Fig. 12.

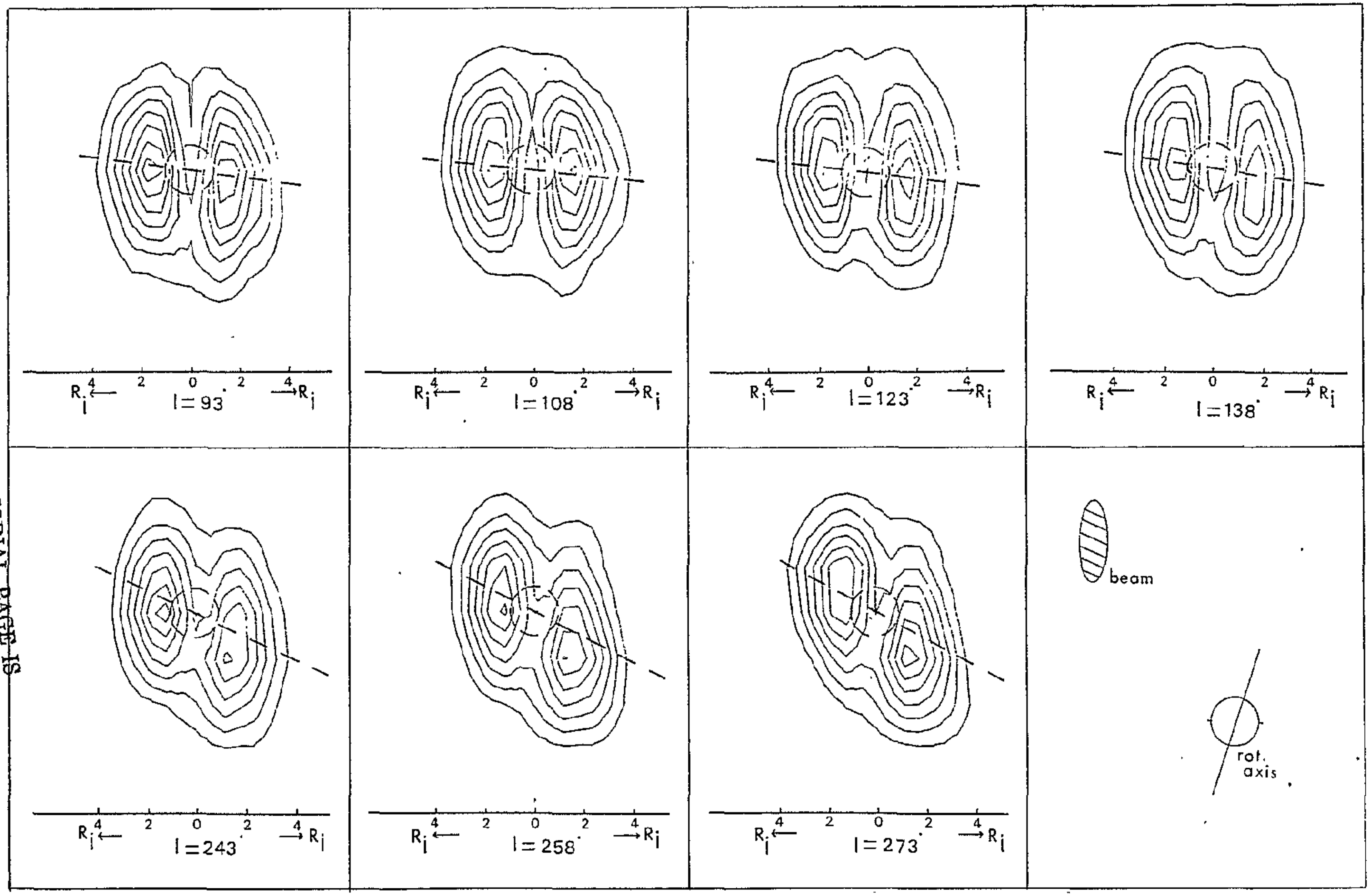

Fig.10

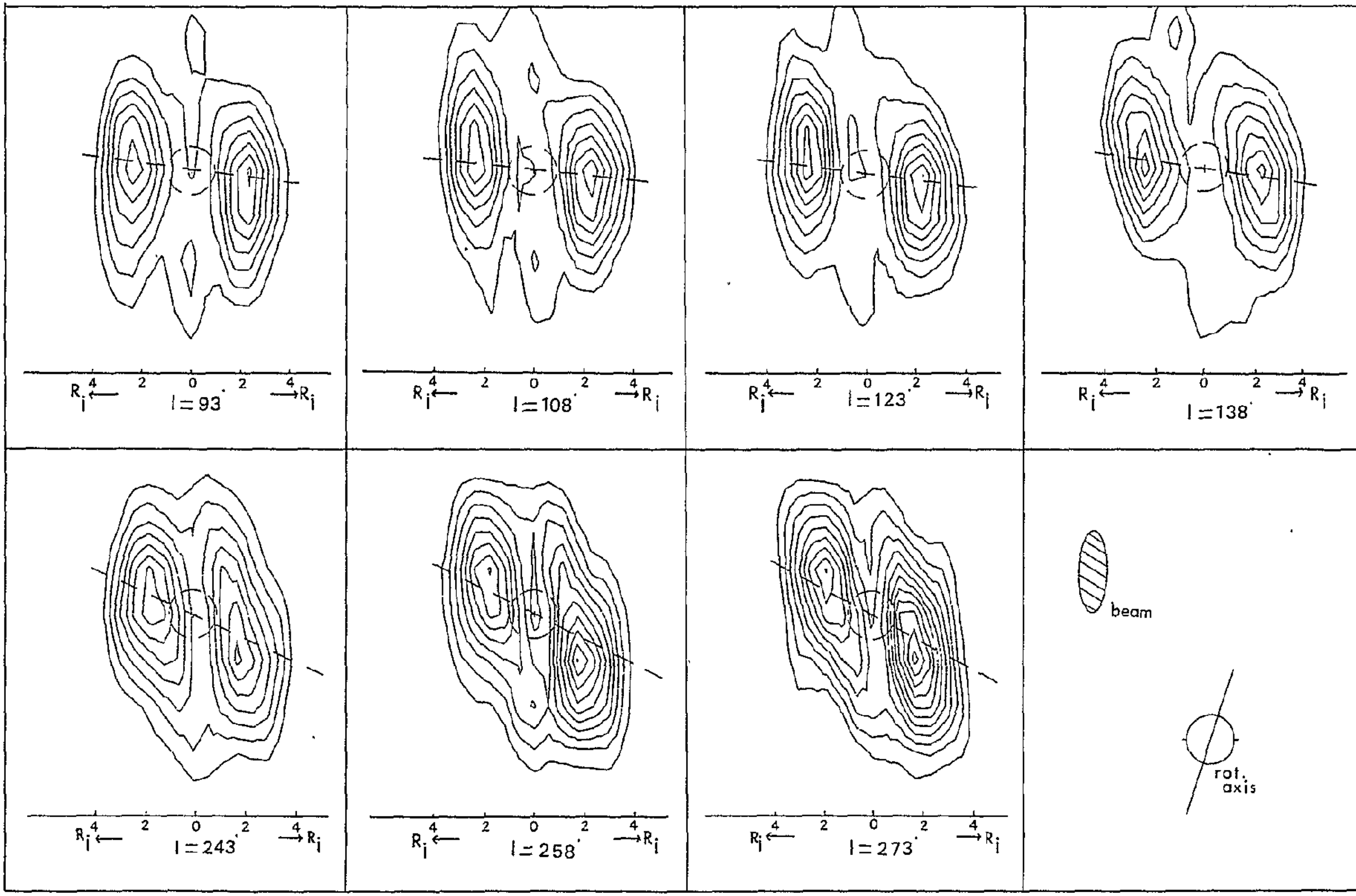

PRECEDING PAGE BLANK NOT FILMED

Fig. 12

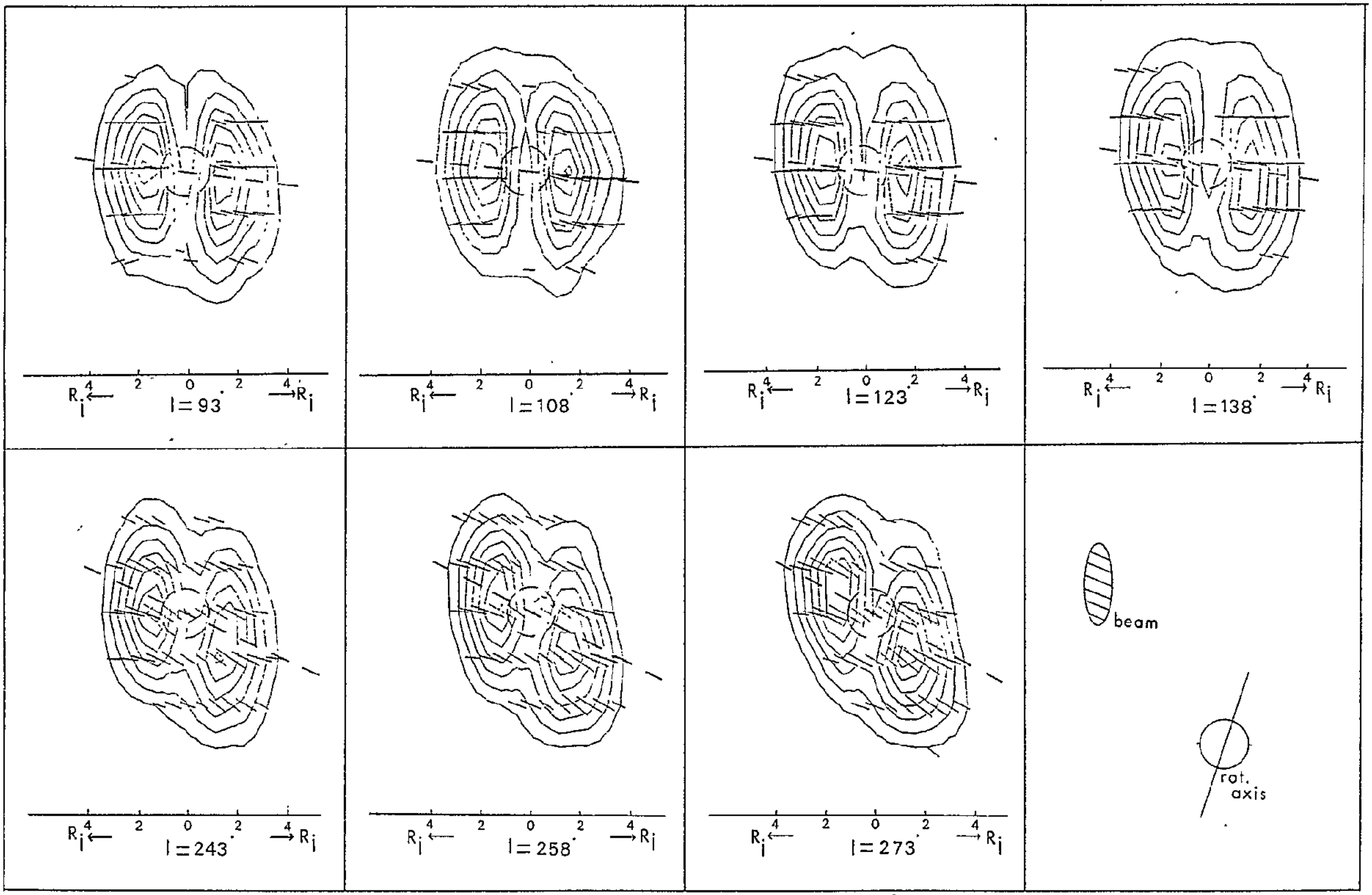

Rj 4 2 0 2 4 Rj
l = 93°
Rj 4 2 0 2 4 Rj
l = 108°
Rj 4 2 0 2 4 Rj
l = 123°
Rj 4 2 0 2 4 Rj
l = 138°
Rj 4 2 0 2 4 Rj
l = 243°
Rj 4 2 0 2 4 Rj
l = 258°
Rj 4 2 0 2 4 Rj
l = 273°
beam
rot. axis

Fig. 13

4.4 Convolved Jovian maps.

Comparing maps of a source at different wavelengths it is necessary that they have about equal resolution. In fact it would be fairest when the datapoints would lie in the same part of the UV plane. We therefore neglected all interferometers at the shorter wavelength with baselines $\frac{L}{\lambda s} > \frac{L_{max}}{\lambda l}$, where s and l refer to the shorter and longer wavelength respectively and L_{max} is the maximum baseline used at λ_1. It was not necessary to leave out the interferometers at λ_1 with baselines $\frac{L}{\lambda l} < \frac{L_{min}}{\lambda s}$, since it did not produce any difference in our maps. Fourier transforming the datapoints left from the observati[on] we increased the distance between two gridpoints with factors of 2, 4 and 8 for the convolved maps of 21 — 50 cm, 6 — 21 cm and 6 — 50 cm respectively. Then again we have 2 to 2.5 points per half power beamwidth where this width refers to the maximum baseline left in the observation.

One of the disadvantages of leaving out interferometers is the increase in noise with a factor $\sqrt{\frac{N_1}{N_2}}$ where N_1 = 20 the total number of interferometers and N_2 is the number used.

N_2 = 6 for 6 — 21 cm convolution

N_2 = 3 for 6 — 50 cm

N_2 = 9 for 21 — 50 cm

Convolution of 6 — 21 cm.

Fig. 4.14 shows a map of the total radiation at 6 cm convolved to 21 cm. The real noiselevel increases with a factor of 2 in doing this, but from the map I would estimate an uncertainly level of about 250 mJy/beam. The belts. This particularly is shown at the right hand side of the picture. At the left side negative ridges, remnants of the true antennapattern were left in the map after having "cleaned" it. This distorts the source at that side. The elongation in declination is due to the beamwidth in that direction.

At 50 cm there is no resolution at all in declination. We therefore made only one dimensional stripscans of the 6 — 50 cm and 21 — 50 cm data as shown in Fig. 4.15 and 16. The 21 cm scans are similar in shape as the 50 cm scans from Fig. 4.5 and they have an uncertainty level of nearly 125 mJy/beam. The 6 cm scans I dare not trust entirely; the uncertainty level is about 200 mJy/beam in the upper pictures (6 — 21 cm) and 400 mJy/beam at the lower scans (6 — 50 cm). Looking at the upper scan at 48^{o} also the positional accuracy does not look trustworthy (which was even worse at all other scans at this wavelength). I therefore did not use the total flux from these scans nor the distribution over the two sides of the belt (see i.e. the scan at $\lambda = 93^{o}$ which shows a maximum intensity at the other side of the disk than the one at 21 cm does; what to think of it?).

A comparison of the scans convolved to 50 cm after subtraction of a thermal disk of 236K at 6 cm and 290K at 21 cm with those at 50 cm (where a thermal flux of 0.1 Jy was subtracted which corresponds to $\sim$ 265K shows that the width of the emission region R_e increases with wavelength roughly as $R_e \sim \nu^{-0.1}$ (where ν is the frequency). The fact that it increases was not unknown before. It indicates that the lower energy electrons which radiate at longer wavelengths (assuming a dipole-like configuration with sizes as measured at the various frequencies) have mean orbital distances farther off the center than the higher energy electrons. This is similar to the

situation found for the earth's radiation belts (Søraas, 1973).
The ratio of the degrees of the integrated linear polarization at 50 cm to 21 cm is 0.9 ± 0.15. The integrated position angles of the electric vector are about equal at both wavelengths, which confirms the idea that there is hardly any depolarization nor Faraday rotation in the source.
The spectral index of the synchrotron component (defined such that S_ν = Const. $\nu^{-\alpha}$) of the integrated emission between 21 and 50 cm appears to be about α = 0.08 ± 0.05 which implies a mean energy spectrum of electrons in this range of about

$$N(E)\ dE \sim E^{-1.16}\ dE$$

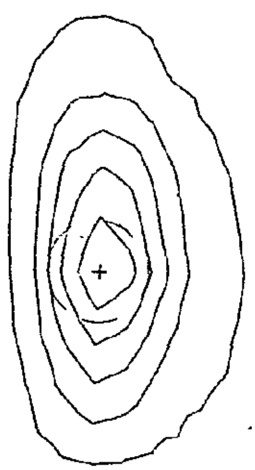

Fig. 4.14 A map at 6 cm convolved to 21 cm.
Contour values are: 0.5 – 7.5 Jy/beam in steps of 1 Jy/beam.
The planetary disk is indicated by the dotted circle.

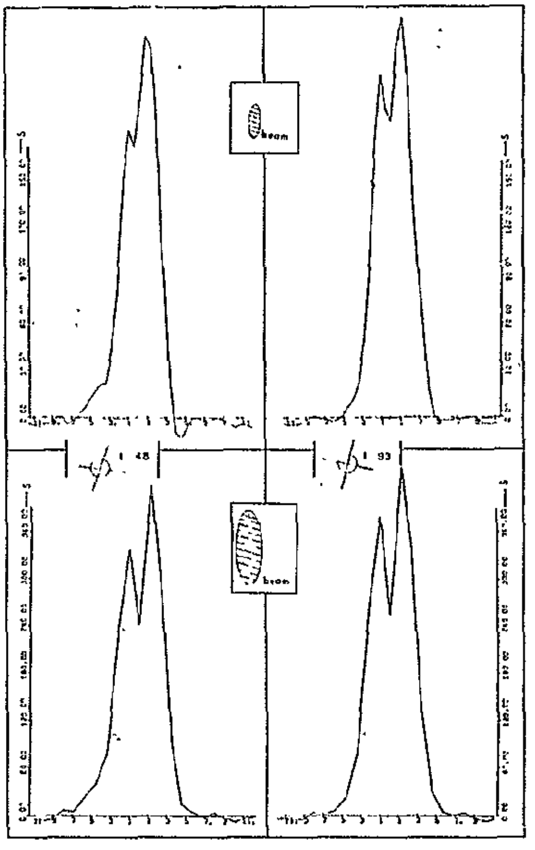

Fig. 4.15 Stripscans at 6 cm convolved to 21 cm (upper two scans) and to 50 cm (lower two scans).

For further details see caption of Fig. 4.2.

ORIGINAL PAGE IS OF POOR QUALITY

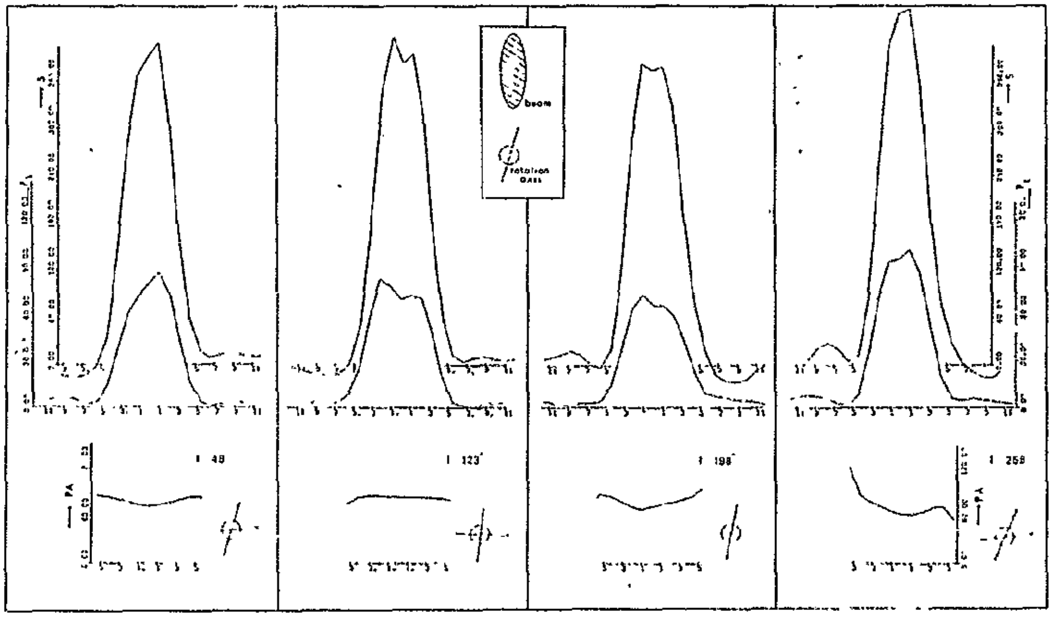

Fig. 4.16 Stripscans at 21 cm convolved to 50 cm. See also caption of Fig. 4.2

4.5 Conclusions.

The main results from this work are the following:

Thermal radiation:

a) The thermal disk of Jupiter measured at a wavelength of 6 cm has a temperature of 236 ± 15 K.

b) There may be some limb darkening over the planetary disk at 6 cm.

c) The temperature of the thermal disk at 21 cm appears to be about 300 - 320 K (with lower and upper limits of 270 and 360 K respectively).

d) The ammonia mixing ratio may be a factor of 4 to 5 larger than the solar value of 1.5×10^{-4}.

Non-thermal radiation:

e) The radiation belts have an overall structure governed by the trapping of electrons in the dipolar field of the planet with significant beaming of the synchrotron radiation into the plane of the magnetic equator.

f) The total flux received is less than the fluxes received a few years earlier, but in agreement with the level obtaining after the sudden decrease in
in 197

g) A comparison of our scans with Berge's 10.4 cm scan observed prior to 1972 showed a decrease in the distance from the disk center to the flux p

h) There exists a hot region in the radiation belts with

1. a position of λ_{III} (1965.0) = $255^{\circ} \pm 10^{\circ}$
2. a flux of 0.4 Jy which is 9% of the total non-thermal flux,
3. an extent of about 50° in longitude and a volume emissivity enhance a factor of ~ 1.6 with respect to the general radiation belts,
4. the position of this hot region may be drifting with time.

i) The lower frequency (longer wavelength) emission comes from further ou in the radiation belts implying that the lower energy particles are farth away from the center (assuming a dipole-like configuration with sizes as

j) The spectral index of the integrated synchrotron radiation between 21 cm and 50 cm is +0.08 ± 0.05.

In the near future we shall try to get more accurate pictures with the Westerbork telescope at all three wavelengths at a much higher declination for all rotational aspects of the planet. With these we hope to solve most of the mysteries concerning the hot region and to check again the thermal disk temperatures at 6 cm and 21 cm. At 21 cm we will also try to map the circular polarization component which will be of great help in unraveling the magnetospheric structure. With a better signal to noise ratio we should be able to detect the characteristics of the non-thermal synchrotron emission at 6 cm.

References.

Baars, J.W.M., Hooghoudt, B.G. 1974: Astron. & Astrophys. 31, 323

Beard, D.B. and Luthey, J.L., 1973: Astrophys. J. 183, 679

Berge, G.L., 1966: Astrophys. J. 146, 767

Berge, G.L. and Gulkis, S., 1976: in Jupiter, p. 655. Ed. T. Gehrels, University of Arizona Press, Tucson, Arizona.

Branson, N.J.B.A., 1968: Mon. Not. Roy. Astron. Soc. 139, 155

Brouw, W.N., 1971: Ph.D. dissertation. University of Leiden, The Netherlands

Brouw, W.N., 1975: Methods in Comput. Phys. 14, 131.

Casse, J.L. and Muller, C.A., 1974: Astron. & Astrophys. 31, 333

Conway, R.G. and Stannard, D., 1972: Nature Phys. Sci. 239, 142.

Degioanni, J.J., 1973: Ph.D. dissertation. University of Illinois. Urbana, Illinois.

Gardner, F.F. and Whiteoak, J.B., 1977: Astron. & Astrophys. 60, 369

Goodman, G.C., 1969: Ph.D. dissertation. University of Illinois. Urbana, Illinois.

Gulkis, S., 1973: Space Sci. Rev. 14, 497.

Högbom, J.A., 1974: Astron. & Astrophys. Suppl. 15, 417

Högbom, J.A., and Brouw, W.N., 1974: Astron. & Astrophys. 33, 289.

J. Geoph. Res. 79, (1974) Special issue concerning the Pioneer 10 mission:

Smith, E.J. et al, p. 3501.

Simpson, J.A., et al, p. 3522.

van Allen, J.A. et al, p. 3559.

Klein, M.J., 1975: Nature 253, 102

Larson, H.P., Fink, U., Treffers, R., Gathier III T. N., 1975: Astrophys. J. 197, L 137.

Lewis, J.A., 1969: Icarus 10, 365

Luthey, J.L. and Beard, D.B., 1973: Astrophys. J. 183, 671.

Neidhöfer, J., Booth, R.S., Morris, D., Wilson, W., Biraud, F., and Ribes, J.C., 1977: Astron. & Astrophys. 61, 321.

Roberts, J.A., 1976: Proc. Astron. Soc. Australian 3, 53.

Van Someren Greve, H.W., 1974: Astron. & Astrophys. Suppl. 15, 343.

Søraas, F., 1973: in Cosmical Geophysics, Ed. A. Egeland, Ø. Holter and A. Omholt. Universitetsforlaget, Oslo-Bergen-Tromsö.

Tomasko, D., Dickel, J.R. and Goodman, G.C., 1974: B.A.A.S. vol. 6, p. 377.

Wallace, L., and Hunten, D.M., 1977: Rev. Geophys. and Space Phys., in press.

Weiler, K.W., 1973: Astron. & Astrophys. 26, 403.

Weiler, K.W. and Raimond, E., 1976: Astron. & Astrophys. 52, 397.